Global and Planetary Change 253 (2025) 104949

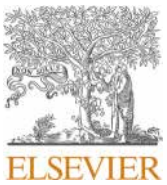

Contents lists available at ScienceDirect

Global and Planetary Change

journal homepage: www.elsevier.com/locate/gloplacha

Contrasting short-term dynamics of supraglacial ponds along the Hindu Kush-Himalaya revealed by PlanetScope imagery and deep learning

Xingyu Xu [a,*], Lin Liu [a], Lingcao Huang [b], Yan Hu [a,c], Guoqing Zhang [d], Adina Racoviteanu [e], Emily Victoria Liu [a], YingTo Agnes Chan [a]

[a] Department of Earth and Environmental Sciences, Faculty of Science, The Chinese University of Hong Kong, Hong Kong, China
[b] Institute of Space and Earth Information Science, The Chinese University of Hong Kong, Hong Kong, China
[c] Institute of Environment, Energy and Sustainability, The Chinese University of Hong Kong, Hong Kong, China
[d] State Key Laboratory of Tibetan Plateau Earth System Science, Environment and Resources (TPESER), Institute of Tibetan Plateau Research, Chinese Academy of Sciences, Beijing, China
[e] University Grenoble Alpes, IRD, CNRS, INRAE, Grenoble INP, IGE, F-38000 Grenoble, France

ARTICLE INFO

Editor: Dr. Jed O. Kaplan

Keywords:
Supraglacial ponds
Deep learning
PlanetScope imagery
Glaciers
Hindu Kush-Himalaya

ABSTRACT

An increasing number of supraglacial ponds have formed and expanded on the surface of debris-covered glaciers across the Hindu Kush-Himalaya (HKH) mountain range in the last decades. Despite the pronounced spatio-temporal variability observed in supraglacial ponds at annual and decadal scales, investigations of their seasonal changes are limited over large spatial scales. These investigations are critical for evaluating their impacts on glacier ablation and dynamics and predicting water resource availability. Here, we produced detailed seasonal maps of supraglacial ponds at five sites of the HKH for the years 2017 to 2022 using a deep-learning-based mapping method applied to PlanetScope imagery. Using these maps, we investigate pond seasonality and interannual variability. We found that (1) the average pond number and percentage ponded area over the debris-cover area were higher in the Central Himalaya (417, 1.55%) and Eastern Himalaya (481, 1.93%) compared to those in the Hindu Kush (142, 0.20%) and Western Himalaya (153, 0.19%); (2) pond percentage area over debris-cover area showed an increase in the Karakoram (+0.2% in an absolute sense), Central Himalaya (+0.6%) between 2017 and 2020, and Eastern Himalaya (+0.9%) between 2018 to 2021; (3) supraglacial ponds reached their peak at the onset of the ablation season (May-June) in the Karakoram and the Hindu Kush, during the pre-monsoon season in the Western and Central Himalaya, and during the monsoon or post-monsoon period in the Eastern Himalaya; (4) the Central Himalaya displayed a highest occurrence of persistent ponds (17.2%), while only 4.3% of supraglacial ponds in the Karakoram were persistent. Our results provide a spatially diverse and temporally detailed dataset that serves to advance the understanding of supraglacial pond dynamics across the Hindu Kush-Himalaya.

1. Introduction

The Hindu Kush-Himalaya (HKH) mountain range, containing the world's largest ice and snow outside the polar regions, is home to ~40,000 glaciers, with a total area of ~60,000 km^2 (Dyurgerov and Meier, 2005). With the progressive mass wastage of debris-covered glaciers (DCG) in the HKH (Kääb et al., 2012; Thompson et al., 2016), an increasing number of supraglacial ponds have been forming and expanding in the recent decades (Bolch et al., 2008; Nie et al., 2017; Khadka et al., 2018; Chand and Watanabe, 2019), partly due to meltwater accumulating within depressions on low-sloping (<10°), stagnant surfaces of glaciers (Sakai and Fujita, 2010; Benn et al., 2012; Thompson et al., 2016). These ephemeral supraglacial water bodies originate from 'perched' ponds situated above the hydrological base-level (Benn et al., 2012). Over time, some of these ponds evolve, deepen and drain once they become connected to the en- or sub-glacial drainage systems (Benn et al., 2012). Other fast-developing ponds coalesce, forming large supraglacial lakes that ultimately may evolve into proglacial lakes (Benn et al., 2012; Thompson et al., 2012), posing concerns for glacier lake outburst floods.

Supraglacial ponds are important meltwater storage reservoirs, effectively modulating glacial runoff and the timing and availability of

* Corresponding author.
E-mail address: xuxingyu@link.cuhk.edu.hk (X. Xu).

https://doi.org/10.1016/j.gloplacha.2025.104949
Received 3 September 2024; Received in revised form 16 June 2025; Accepted 19 June 2025
Available online 21 June 2025

meltwater to downstream communities (Irvine-Fynn et al., 2017). These ponds facilitate basal sliding and increasing glacier velocity through water infiltration into the englacial system (Watson et al., 2016; Miles et al., 2017a; Wendleder et al., 2021). As local "hot spots" of ice melt, supraglacial ponds can enhance glacial ablation rates by a factor of 14 ±3 (Miles et al., 2018). Additionally, they facilitate heat transfer to subaqueous ice and contribute to potentially up to 1/8 of the catchment ice mass losses (Sakai et al., 2000; Miles et al., 2016; Mertes et al., 2017; Miles et al., 2018; King et al., 2019; Racoviteanu et al., 2022). Furthermore, the evolution of supraglacial ponds into proglacial ice or moraine-dammed lakes enhances the potential for generating glacier lake outburst floods, posing significant risks to downstream communities (Richardson and Reynolds, 2000; Benn et al., 2012).

Existing studies in the HKH report rapid expansion of supraglacial ponds in recent decades, with high spatiotemporal variability. At a regional scale, several studies report larger ponds and higher expansion rates in West Nepal (Everest region) and Bhutan, versus smaller ponds with lower growth rates in the Hindu Kush and the Karakoram (Gardelle et al., 2011; Nie et al., 2017). However, most of the previous studies on temporal changes were limited to individual ponds/glaciers in well studied catchments in the Nepal Himalaya (Miles et al., 2017b; Steiner et al., 2019; Taylor et al., 2021; Zeller et al., 2024) and focused on decadal scales only in these same regions (Bolch et al., 2008; Watson et al., 2016; Chand and Watanabe, 2019).

Quantifying the spatial-temporal patterns of supraglacial ponds is therefore important, and this requires detailed investigations on the basis of accurate, comprehensive, and multi-temporal supraglacial pond datasets. However, these are lacking over the HKH region due to the highly dynamic behavior and diverse characteristics of these ponds (e.g., irregular shapes, varying sizes, and turbidity) and the limited frequency of measurements over the large extent of the HKH (Chen, 2021). Field studies have been conducted on limited supraglacial ponds such as those on Ngozumpa Glacier in the Khumbu region of Nepal (Benn et al., 2000; Benn et al., 2001; Casey et al., 2012; Qiao et al., 2015). In the last decades, the increased availability of remote sensing data has triggered increased interest in mapping supraglacial ponds, though this was conducted mainly at annual or decadal scales, using Landsat and ASTER data (Wessels et al., 2002; Bolch et al., 2008; Khadka et al., 2018; Gardelle et al., 2011). With the availability of high-resolution optical and radar satellite images such as Sentinel-1, Sentinel-2, WorldView and PlanetScope, recent efforts have also been made to investigate short-term seasonal and inter-annual changes in supraglacial ponds (e.g., Watson et al., 2016; Miles et al., 2017a, 2017b; Narama et al., 2017; Chand and Watanabe, 2019; Taylor et al., 2021; Wendleder et al., 2021).

Various semi-automated algorithms have been used so far, including band ratio or normalized difference water indices (NDWI) (Johansson and Brown, 2013; Watson et al., 2018; Hochreuther et al., 2021), threshold segmentation based on SAR backscatter intensity (Wangchuk and Bolch, 2020), object-based image analysis (Panday et al., 2011; Qiao et al., 2015; Kraaijenbrink et al., 2016; Mitkari et al., 2017) and linear spectral unmixing (Scherler et al., 2018a; Kneib et al., 2021b; Racoviteanu et al., 2021). These allowed mapping supraglacial ponds from various remote sensing datasets in a more time-efficient way, mitigating the time-consuming and labor-intensive manual delineation (e.g., Thompson et al., 2012; Watson et al., 2016; Miles et al., 2017b). However, many of the conventional methods mainly rely on manually-specified features and iterative threshold adjustment, and thus are difficult to apply effectively to large-volume multi-temporal images. Establishing an appropriate threshold value applicable for mapping supraglacial ponds across large regions is challenging due to diversity in the water index caused by pond properties such as turbidity, composition, and depth (Watson et al., 2016). Employing a single threshold of certain index may lead to the exclusion of some supraglacial ponds and the misclassification of features such as clean ice or snow patches, which also exhibit high water index values. Furthermore, some studies have used a fixed lake area threshold as a filter (e.g., 0.0036 km^2 in Gardelle et al., 2011; 0.008 km^2 in Nie et al., 2017; 0.05 km^2 in Shugar et al., 2020), thus overlooking a large number of small-sized supraglacial ponds. Despite significant progress in supraglacial pond mapping, we still lack robust, detailed spatio-temporal characterization of supraglacial ponds across the HKH range.

Deep learning provides a powerful tool for supraglacial pond extraction at multi-temporal spatial scales in a systematic manner. These algorithms automatically extract features from raw data, enabling quick and accurate analysis through parallel processing. Furthermore, deep learning models trained for specific tasks can be adapted for broader applications across various domains using transfer learning (Huang et al., 2022). This capability enhances the accuracy and efficiency of pond mapping by enabling the inference of pond presence across different times and regions. With their high efficiency and transferability, deep-learning-based methods have great potential for effectively capturing the dynamic nature and diverse characteristics of supraglacial ponds across large regions. Specifically, the method of image semantic segmentation, which interprets the image at the pixel level by classifying each pixel into a predefined category, is suitable for delineating supraglacial pond boundaries from satellite images (Qayyum et al., 2020; Wang et al., 2022; Xu et al., 2024). For instance, Yuan et al., (2020) employed a Convolutional Neural Network to extract supraglacial lakes in Southwest Greenland from Landsat-8 imagery. Lutz et al. (2023) developed a deep learning architecture based on U-Net to map supraglacial lakes from Sentinel-2 images over Northeast Greenland. Dirscherl et al. (2021) applied a modified U-Net semantic segmentation model and automatically mapped Antarctic supraglacial ponds on Sentinel-1 Synthetic Aperture Radar (SAR) imagery. Chen (2021) applied a U-Net-based deep learning model to extract supraglacial pond boundaries and other surface features from GaoFen-3 SAR imagery in the Everest region. Despite the significant advantages that deep-learning-based methods offer in mapping supraglacial ponds, it is essential to recognize that they do have certain limitations, which include: (1) ineffectiveness in identifying small and elongated supraglacial ponds (Chen, 2021); (2) occurrence of false predictions on shadows.

This study addresses these challenges, by improving existing techniques to better map supraglacial ponds with the goal of investigating short-term variations of supraglacial ponds over several regions in the HKH. Specifically, our objectives are: (1) to produce a systematic deep learning technique that can map supraglacial ponds automatically and accurately from multi-temporal, high-resolution PlanetScope imagery; (2) to investigate the spatio-temporal variability of supraglacial ponds in five representative sites across the HKH region at seasonal scales for the period 2017 to 2022 and (3) to quantify and compare the dynamics and persistency of individual supraglacial ponds at regional scale. We investigate the short-term dynamics and the regional heterogeneities of supraglacial ponds, and assess the climatic factors (such as temperature and precipitation) and glacier settings that may affect these dynamics at regional scales.

This paper is organized as follows. Section 2 introduces the location, climatic setting, and key glacier characteristics of our study area. Section 3 details the datasets and methodologies employed to map supraglacial ponds, quantify their spatio-temporal changes, and track the dynamics of individual ponds. Section 4 presents our findings, including mapping accuracy, a comparative analysis of pond distribution and seasonal variation patterns across the five study areas, and insights into the dynamics of individual ponds. Section 5 critically evaluates the strengths and limitations of our mapping approach and explores the potential factors underlying the observed distinct patterns of pond distribution and change.

2. Study area

Our study areas are situated within the HKH region, which extends 3,500 km and covers a total area of 3,441,719 km^2 (Sharma and Partap,

1994). Due to the size of the domain and the large amount of data needed to cover it, we selected five study sites (~2000 km^2 each) based on percentage debris cover and pond abundance distributed across the HKH regions: the Hindu Kush, the Karakoram, the Western, Central and Eastern Himalaya (Fig. 1). While we acknowledge that the study sites may not fully capture the diversity of the entire sub-region due to local variability, they serve as indicative samples, exhibiting a broad range of elevations and sharing comparable distributions in terms of area, slope, and glacier velocity with those spanning the entire subregion (Figure S1). For the sake of simplicity, we used the larger sub-region name to refer to our study areas in the remainder of the paper.

These sites are situated under different climatic conditions, which are linked to the occurrence of the Indian Summer monsoon (Bookhagen and Burbank, 2006). The east-west gradient in monsoon intensity causes differences in temperature, precipitation, and humidity across the HKH, influencing glacier dynamics, mass balance and glacio-hydrological patterns. The Central and Eastern Himalaya regions experience large amounts of precipitation during the monsoon period (~ June to late September) (Bookhagen et al., 2005). The intensified rainfall during the monsoon season acts as one of the water inputs and modulates the seasonal variation of supraglacial ponds. In contrast, the Hindu Kush and Karakoram regions are influenced by mid-latitude westerlies, which bring large amounts of moisture and snow during the winter (Palazzi et al., 2013).

Glacier mass balance vary among regions. In the Himalayas, glacier mass balance tends to be mostly negative (Kääb et al., 2012; Azam et al., 2018; Hugonnet et al., 2021), with total mass loss rates reaching -0.52 ±0.15 m w.e. yr^{-1} in the Eastern Himalaya, -0.36±0.09 m w.e. yr^{-1} in the Central Himalaya and -0.37±0.09 m w.e. yr^{-1} in the Western Himalaya for the period 2000 to 2018 (Shean et al., 2020). However, glaciers in the Karakoram (-0.04±0.04 m w.e. yr^{-1}) and the Hindu Kush (-0.09 ±0.06 m w.e. yr^{-1}) have experienced relatively stable mass balance during 2000 and 2018 (Shean et al., 2020), although this anomaly is coming to an end (Hugonnet et al., 2021).

Glaciers characteristics vary across the five study sites (Table 1). Supraglacial debris cover is estimated to 14-18% in the Himalayas around the year 2000 (Kääb et al., 2012). Over the last five to six decades, the debris-covered area around the globe, including the Himalayas, has increased due to glacier mass wastage (Scherler et al., 2011; Nuimura et al., 2012; Thakuri et al., 2014; Mölg et al., 2020). Within our study sites, the proportion of debris cover is high in the study areas of Hindu Kush, Western, and Central Himalaya, but lower in the Karakoram and Eastern Himalaya (Table 1). Glaciers in the Hindu Kush, Karakoram and Western Himalaya are generally located at lower elevations with steeper slopes compared to those in the Central and Eastern Himalaya.

3. Data and methodology

3.1. PlanetScope image and auxiliary dataset collection

For this study, we used the PlanetScope images (https://www.planet.com) for mapping supraglacial ponds, leveraging their high spatial resolution (3.7 m pixel size) and daily acquisitions. We obtained the cloudless images (filtered with cloud cover < 5%) for the five sites at seasonal intervals spanning 2017 to 2022. After visual inspection, we manually selected high-quality images, i.e., where debris-covered area was minimally obscured by mountain shadows, cloud or snow cover (data description in Supplemental Table S1). PlanetScope surface reflectance product offers atmospherically-corrected 4-band imagery comprising Band 1: Blue (455-515 nm), Band 2: Green (500-590 nm), Band 3: Red (590-670 nm), and Band 4: near-infrared (NIR) (780-860 nm). We generated RGB color composites (Band 321) and NDWI using the formula (Green – NIR)/(Green + NIR), both on a seasonal basis for each study site. NDWI exhibits a distinct spectral contrast between water and the surrounding debris cover, and therefore is commonly used to map water bodies including supraglacial ponds with low turbidity or frozen surface (Watson et al., 2018).

We defined the seasons based on the Indian Summer Monsoon and the Westerlies climatic patterns, as follows: for the Hindu Kush and Karakoram study sites, we selected images over three periods: beginning (May-June), mid (July-August) and end (September-October) of the ablation season. For the monsoon-influenced Himalayan region, we selected images from four seasons: pre-monsoon (March 1 to June 15), monsoon (June 16 to September 30), post-monsoon (October 1 to November 30), and winter (December 1 to February 28) if snow-free

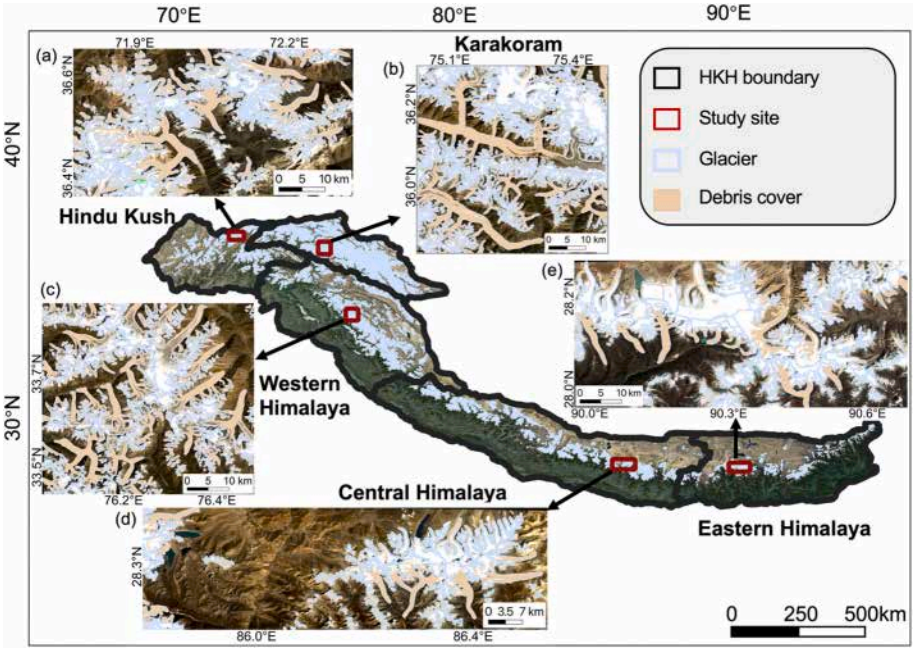

Fig. 1. Glacier distribution across the HKH, showing clean glacier (blue) and supraglacial debris cover (tan) at the five sites with PlanetScope images acquired in October 2022 as background image.

Table 1
Glacier characteristics of the five selected sites based on RGI 7.0 glacier boundaries (RGI 7.0 Consortium, 2023), supraglacial debris cover for the period 2013 to 2017 from Scherler et al. (2018b) and glacier velocities in 2018 from ITS_LIVE (Gardner et al., 2019).

Study site	Total area (km^2)	Glacierized area (km^2)	Percent glacierized area (%)	Debris cover area (km^2)	Percent debris cover (%)	Mean Elevation (m)	Mean Slope (°)	Mean glacier velocity (m/yr)
Hindu Kush	1940	524.77	27.04	179.96	34.29	5255	29.9	22
Karakoram	2074	1686.16	81.29	302.21	17.92	5183	34.6	110
Western Himalaya	1993	862.70	43.30	233.56	27.07	4928	29.2	27
Central Himalaya	2045	512.50	25.05	135.14	26.37	5872	24.0	12
Eastern Himalaya	2057	851.48	41.40	124.45	14.62	5702	21.4	25

images were available following the similar season setting employed by Miles et al. (2017b). For each site, suitable images were mosaicked for each season, preferably within a single month, and supplemented with images from other months within the 3-month seasonal window to ensure full coverage. Within each seasonal time frame, we selected the most recent image to compile the mosaics if multiple images are available. The seasonal mosaic RGB image and mosaic NDWI images for each study site were used as input data in the deep learning model to map supraglacial ponds.

In addition to the PlanetScope imagery, we collected auxiliary datasets (glacier outlines, glacier velocity, elevation data from a Digital Elevation Model (DEM), debris cover, ERA5 reanalysis dataset) subsequently used for pond mapping and analysis, as listed in Table 2.

3.2. Inventorying supraglacial ponds using deep learning model

We trained the deep learning model (DeepLabv3+) based on RGB and NDWI images separately for delineating supraglacial ponds from multi-temporal PlanetScope imagery at these five sites (Chen et al., 2018). We adopted DeepLabv3+ as the network architecture with Xception-65 as our backbone, a more advanced deep learning architecture than previously used models such as U-Net. In contrast with U-Net which features a symmetric encoder-decoder architecture with skip connections, DeepLabv3+ employs an encode-decode structure with atrous separable convolution to refine segmentation boundaries and extract multi-scale contextual information by adjusting the field of view without losing resolution (Fig. S3) (Chen et al., 2018). DeepLabv3+ has shown successful applications in mapping landforms from satellite images in previous studies (Chen et al., 2018; Huang et al., 2020; Zhang et al., 2021) and outperformance in the PASCAL VOC image segmentation contest. This serves as a benchmark challenge, providing standardized datasets and evaluation metrics for comparing various methods. Fig. 2 shows the flowchart of training and testing the deep learning model, with details described in the following subsections.

Table 2
Auxiliary datasets and their sources for pond mapping and analysis.

Dataset	Source	Usage
Glacier outlines	RGI 7.0 (RGI 7.0 Consortium, 2023)	Define glacier mask and distinguish supraglacial ponds from other water bodies (e.g., proglacial lakes)
Debris cover	Scherler et al. (2018a)	Calculate the percentage ponded area of the debris-covered area and enable comparison with other studies
DEM	Copernicus DEM GLO-30 (European Space Agency, 2024))	Supplementary information for constructing slope profile and removing false predictions by setting slope threshold
Glacier velocity	ITS_LIVE data (Gardner et al., 2019)	Implement ice flow correction for tracking individual supraglacial ponds
Temperature and precipitation	ERA5-Land hourly climate reanalysis dataset (Muñoz-Sabater et al., 2021)	Characterize seasonal changes of temperature and precipitation and investigate the correlation with pond variation

3.2.1. Preparing input data

Input data consisted of training and label images. Training images contain supraglacial ponds from the Eastern Himalaya study site spanning all seasons over five years (2017–2022) to ensure temporal diversity of training data, since pond surface color, shape, and frozen condition may vary over time. We also obtained supraglacial pond labels from Maharjan et al. (2018), Wang et al. (2020), and Chen et al. (2021). To ensure that the label boundaries matched our PlanetScope imagery, we manually delineated 3241 representative and diverse supraglacial ponds in the Eastern Himalaya (referred to as "positive polygons") (Fig. S1). We also mapped 573 non-supraglacial-pond objects such as snow, bare terrain, vegetation, shadows, and glaciers ("negative polygons") and included them in the training sample to reduce false predictions due to similarity of landforms (Table S2). We subsequently created binary (1/0) label images by rasterizing positive and negative polygons with a 300-m buffer area to include contextual information. We divided training and label image patches into training (90%) and validation (10%) to ensure sufficient training samples (Table S2).

To test the deep learning model accuracy and transferability across different sites and seasons, we manually delineated 1,809 supraglacial ponds in the Central Himalaya in 2018 and 1,905 supraglacial ponds in the Karakoram in 2021 based on multi-season RGB and NDWI images and used these as ground truth labels.

3.2.2. Training the deep learning network

We initialized the network using a DeepLabv3+ model pre-trained by the ImageNet dataset, which is a large-scale image database containing over 14 million annotated images across more than 21,000 categories (https://image-net.org/). We fine-tuned the model with RGB and NDWI images separately to test the performance of each approach. We set the learning rate to 0.003, the batch size to 8, and the iteration number to 30000, respectively, as recommended by Chen et al. (2018). During the training process, the predictive model was also applied to the validation datasets and labelled each pixel as a supraglacial pond or non-supraglacial-pond class. We evaluated the model accuracy on the validation datasets by calculating the intersection over union (IoU) between the output raster images and the ground truth label image using the equation:

$$\mathrm{IoU}_{\mathrm{pixel}} = \frac{tp}{tp + fp + fn} \quad (1)$$

where *tp*, *fp*, and *fn* are the numbers of true positive, false positive, and false negative pixels, respectively. We trained the network iteratively until the $\mathrm{IoU}_{\mathrm{pixel}}$ value for the supraglacial pond class reached 0.8 and the mean IoU (mIoU) value of supraglacial pond and non-supraglacial-pond class reached 0.9 (comparable to the performance of the top

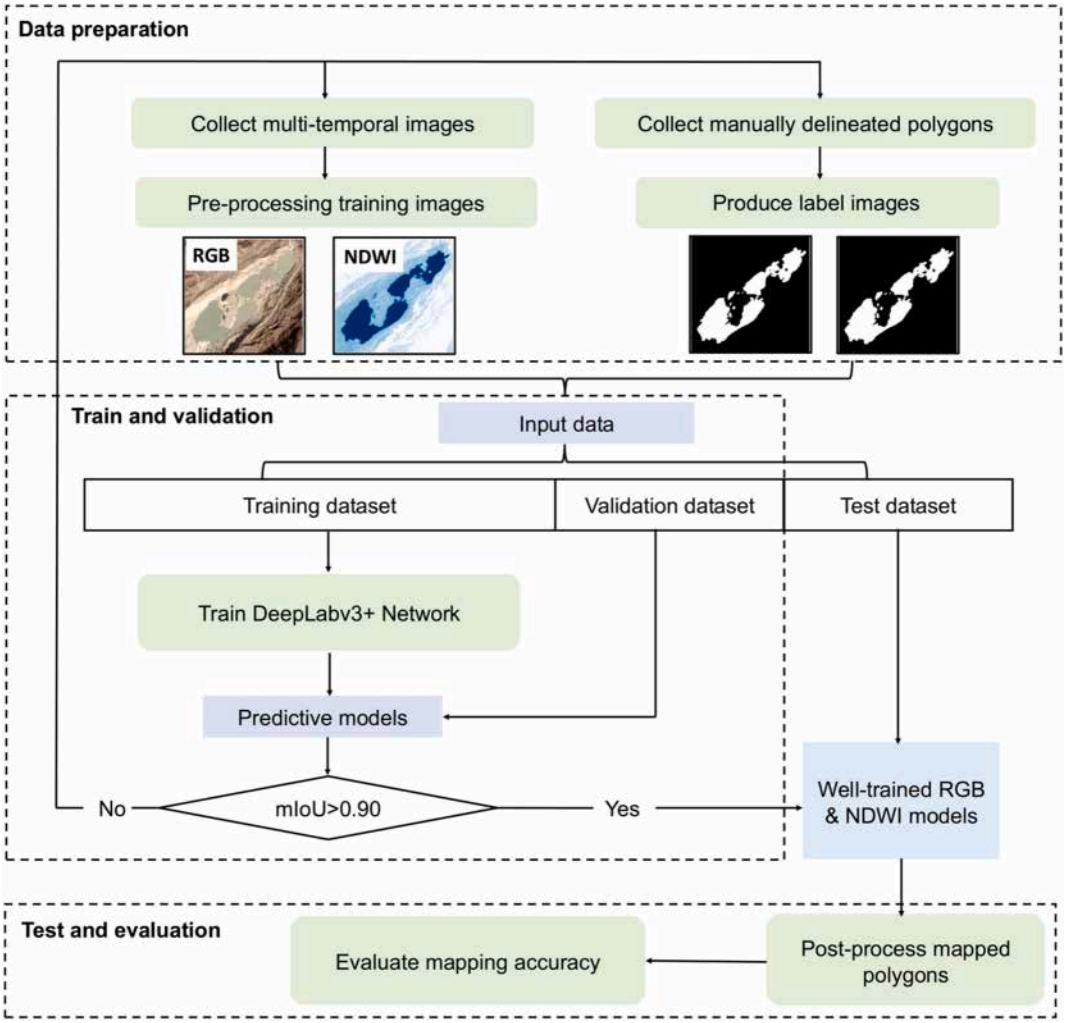

Fig. 2. Workflow of establishing the deep-learning-based mapping method based on RGB and NDWI images, respectively.

models in the PASCAL VOC contest) through enriching the negative training samples, adjusting image augmentation strategies, and fine-tuning hyperparameters.

3.2.3. Post-processing steps and evaluating accuracy

The output of the DeepLabv3+ model was a binary image. We vectorized the inferred supraglacial pond pixels (class 1) to polygons, and performed a series of post-processing procedures to remove false predictions. First, to account for uncertainties in RGI glacier boundaries, we considered any polygon whose intersection percentage with the RGI glacier outlines exceeded 90% to be a supraglacial pond, and the remaining were regarded as other water bodies such as proglacial lakes and were thus removed. We then calculated the mean slope of the mapped pond polygons based on the 30-m resolution Copernicus Global DEM (European Space Agency, 2024). Acknowledging the DEM uncertainties, and the possibility that supraglacial ponds may be situated in areas with relatively high average slopes but low longitudinal gradients (Richardson and Reynolds, 2000; Benn et al., 2012; Miles et al., 2017b), we set a conservative slope threshold (<40°) to reduce false predictions such as shadows due to steep valleys.

Subsequently, we tested and evaluated the detection accuracy of our model on independent test images from sites situated in the Karakoram and Central Himalaya. After post-processing, we calculated the IoU value between deep learning predicted polygon and manual delineated polygon and regarded those with IoU larger than 0.5 as true positives. We used standard metrics such as precision, recall, and F-1 score (Supplementary Text S1) to quantify the detection accuracy of the mapping results. Finally, we estimated the pixel error of the deep learning boundary delineation by calculating the average distance between deep-learning-generated boundaries and manually mapped outlines (Supplementary Text S2). To compare delineation accuracy with human level, we also quantified the manual delineation error by comparing the manually delineated boundaries on ~400 supraglacial ponds among three experts (Supplementary Text S2).

We applied our trained deep-learning model to map supraglacial ponds over the five sites and generated seasonal maps. To ensure high product quality, we visually inspected and manually refined the mapping results by (1) removing any misclassified supraglacial ponds due to image artifacts and inaccurate glacier outlines, (2) splitting polygons covering more than one supraglacial pond, (3) merging multiple polygons covering the same pond, and (4) retrieving polygons missed due to cloud cover, mountain shadow, snow cover, frozen surface, slope threshold setting, and inaccurate glacier outlines. In the compilation step, we adopted the mapped polygon from NDWI images unless the supraglacial ponds were missed from the RGB images, or when mapped pond boundary was incomplete.

3.3. Quantifying spatio-temporal variations of supraglacial ponds

We reported the total ponds and calculated the total pond area per site and the percentage ponded area (defined as percentage of the total debris-covered area occupied by supraglacial ponds) based on

supraglacial debris cover from Scherler et al. (2018a). We estimated the areal uncertainties of individual ponds using the pixel error multiplied by the pond perimeter and image spatial resolution (Zhang et al., 2021).

Pond density maps (pond counts divided by glacier area in $0.025^\circ \times 0.025^\circ$ grids) were generated based on the seasonal pond maps. We also analyzed pond distribution with respect to their area, elevation, glacier velocity (Gardner et al. (2019), and distance from the glacier termini.

Annual and seasonal time series for both pond number and percentage ponded area across the five study sites were used to investigate pond seasonality and interannual variability. The annual time series, derived primarily from our mapping results for October, minimized the potential impact of monthly variations on evaluating and comparing interannual pond dynamic trends. We performed site-specific assessments, taking into account the regional climatic conditions when characterizing seasonal patterns. In the Hindu Kush and Karakoram regions, we analyzed pond variation throughout the onset, middle, and end of the ablation season. In the Himalayan sites, we tracked pond changes through pre-monsoon, monsoon, post-monsoon, and winter periods.

3.4. Tracking the dynamics of individual ponds

We first implemented ice flow correction on the generated seasonal maps following Kneib et al. (2021a) and Zeller et al. (2024) to identify unique supraglacial ponds and track pond dynamics across the five study sites. Specifically, we shifted the pond position to the earliest acquisition time in June 2017 based on glacier surface velocity from ITS_LIVE data (Gardner et al., 2019). Subsequently, we compared each seasonal pond map with the corresponding previous observations to assess the pond dynamics, quantifying events such as appearance, disappearance, expansion, shrinkage, merging, and splitting for each observation time (Fig. S4). These change events were categorized into two groups for analysis. Group 1 encompasses events such as appearance, expansion, and merging, which contributed to pond growth. Group 2 includes events such as disappearance, shrinkage, and splitting, which lead to pond decline.

We compared the spatial overlap of ponds across seasons during 2017 and 2022, considering overlapping ponds as repeated detections and counting only non-overlapping pond polygons as unique features. This approach accounted for the dynamic nature of supraglacial ponds and enabled a conservative estimation of the total number of distinct supraglacial ponds within each study area over the investigation period.

For each unique supraglacial pond, we further calculated the pond frequency through the study period and classified the ponds into three categories: ephemeral supraglacial ponds (observed in less than half of total observations with pond frequency lower than 0.5), persistent supraglacial ponds (observed in more than half of total observations with pond frequency exceeding 0.5) and permanent supraglacial ponds (observed from every seasonal map with pond frequency of 1). We then compared the number of different types of supraglacial ponds and analyzed the topographic (elevation) and glacial settings (velocity, distance to glacier termini) for each category of supraglacial ponds at five study sites.

4. Results

In this section, we first present the mapping performance of our deep learning method in Section 4.1. Section 4.2 provides a summary of our observed spatial-temporal changes of supraglacial ponds across the five sites. October 2022 is used as a common time window to provide a comparative analysis of supraglacial pond distribution across the five study sites in Section 4.3. Section 4.4 gives site-specific analyses of the interannual and seasonal variations of supraglacial ponds. Finally in Section 4.5, we present the time series of pond change events and report the statistics of pond frequency across five study areas.

4.1. Mapping accuracy of the deep-learning method

The mapping accuracy of the RGB-based model and NDWI-based model are comparable in terms of pixel-based IoU metrics (Table 3); the IoU_{pixel} curve throughout the training process is shown in Fig. S5. The mean IoU_{pixel} values for both RGB-based and NDWI-based models reached 0.91 after iterative training. The F1 scores of RGB-trained model ranged from 0.55 to 0.72 on test images obtained from Central Himalaya across various seasons (Table S3). In the Karakoram, the F1 scores of RGB-trained model ranged from 0.62 to 0.78 (Table S4), generally higher than those of the NDWI-trained models (Fig. S6). The average pixel error of the deep learning mapped boundaries from RGB images was 1.41 pixels (~5.2 m), comparable to the average manual delineation error of 1.38 pixels (~5.1m). The average pixel error of the deep learning mapped boundaries from NDWI images was 1.73 pixels. Consequently, the deep learning model trained on RGB images demonstrated a superior capability for identifying supraglacial ponds in terms of both number and boundary (Fig. S7).

Our deep learning model successfully mapped supraglacial ponds with high turbidity, shadow cover, frozen ponds, and intricate shapes (Fig. 3). Both the RGB and NDWI trained models accurately delineated the boundaries of turbid ponds (Fig. 3a–c) and ponds partially covered by shadow (Fig. 3d–f). However, 69% of the small supraglacial ponds with extremely bright appearance were missed by the RGB-trained model in the zoom-in area (Fig. 3h), while 92% of them were identified by the NDWI-trained model (Fig. 3i). Moreover, the ponds with complex boundaries were accurately identified by the RGB-based model (Fig. 3k). The mapping results based on RGB images therefore served as the primary data source for compiling the final pond maps.

4.2. Overview of spatial-temporal variation of supraglacial ponds across the HKH during 2017- 2022

The characteristics of supraglacial ponds for each study site are summarized in Table 4. Supraglacial ponds in the eastern sites (Central and Eastern Himalaya) exhibited higher percentage ponded area and density, as well as more variable seasonal changes compared to those in the western sites (Western Himalaya and Hindu Kush). Supraglacial pond area increased from 2017 to 2022 across all study sites except in the Hindu Kush. Notably, the Karakoram site exhibited the largest proportions of ephemeral ponds (95.7%, Table 4) and ponds smaller than 0.001 km^2 (42%, Fig. S9).

4.3. Spatial distribution of ponds across the HKH in October 2022

Our deep learning approach enabled the generation of seasonal pond maps across the five study sites. For simplicity and clarity and intercomparison among sites, here we present the pond density maps generated for the reference period of October 2022 (Fig. 4) with the pond maps shown in Fig S8. This month was specifically selected to capture the ablation season across the five sites when images were cloud-, shadow-, and snow-free. In this month, supraglacial ponds covered more than 1.49% of the debris-covered area in the Central and Eastern Himalaya, which was ~8 times greater than in the Hindu Kush and Western Himalaya, and 5 times greater than in the Karakoram (Table 5). Additionally, the average supraglacial pond density was significantly higher in the Central Himalaya (1.5 ponds/km^2) compared to other sites (< 0.68 ponds/km^2). In the Central and Eastern Himalaya,

Table 3
IoU_{pixel} values of background class and supraglacial pond class of the trained deep-learning DeepLabv3+ models.

	IoU_non-supraglacial-pond	IoU_supraglacial pond	Mean IoU
RGB-based	0.995	0.825	0.910
NDWI-based	0.995	0.817	0.906

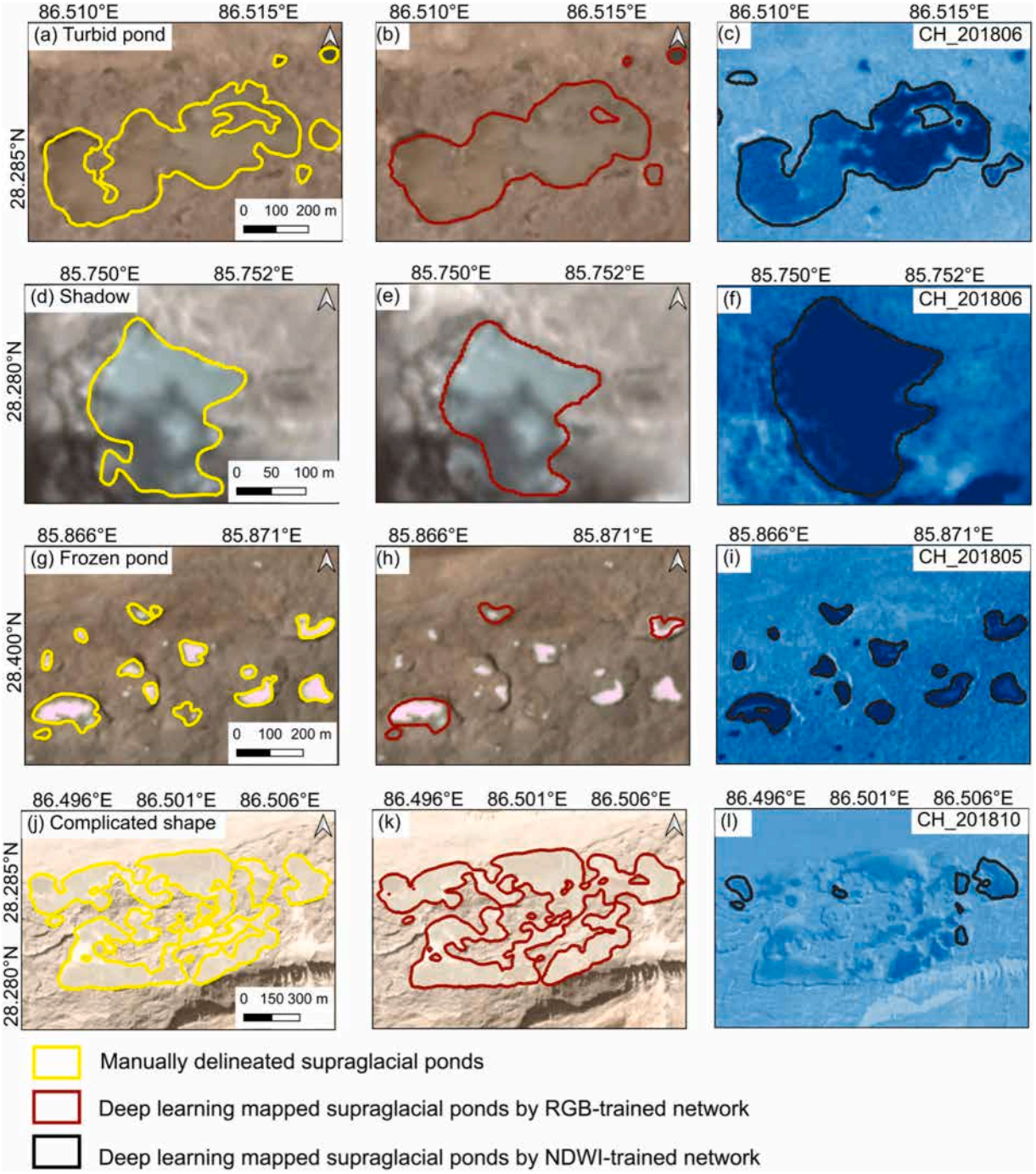

Fig. 3. Examples of the mapping results on turbid ponds (a–c), ponds covered by cloud shadow (d–f), frozen ponds (g–i), and ponds with complicated shapes (j–l) in the Central Himalaya (CH) produced by the deep learning models trained separately using RGB and NDWI images, and the mapped ponds based on manual delineation.

the pond distribution exhibited high spatial heterogeneity, with localized concentration observed at glacier termini, where pond density reached 20-24 / km^2 (Fig. 4).

Approximately 70% of supraglacial ponds were located on the lower part of the glaciers within the normalized distance of 0 to 0.4 from the glacier termini, with a decrease in the total pond area towards the glacier upper sections (Fig. 5) across the five study sites. In contrast, in the Central and Eastern Himalaya, more than 40% of supraglacial ponds are located in the middle to upper sections, with the normalized distance from the glacier termini of 0.4 to 0.8; but their total area is relatively lower than those near the glacier termini (Fig. 5d&e, Fig. S10). We observed large supraglacial ponds (> 0.1 km^2) at the stagnant glacier terminus at these two sites compared to the other three (Figs. S11&S12).

Across the Himalayan sites, approximately 90% of supraglacial ponds are distributed in areas with low glacier velocities (0-20 m/yr) (Fig. 5b). In contrast, 35% of supraglacial ponds at the Karakoram site are situated in areas with glacier velocities exceeding 50 m/yr; this anomaly will be further discussed in Section 5.2.

4.4. Interannual and seasonal pond variation from 2017 to 2022

Between 2017 and 2022, the number of supraglacial ponds in

Table 4
Characteristics of supraglacial ponds by study site: spatial distribution, temporal variation, pond change events, and persistency.

Study site	Sec. 4.3 Distribution (average pond density)	Sec. 4.4 Interannual change of percentage ponded area	Sec. 4.4 Seasonal variation	Sec. 4.5 Pond change events	Sec. 4.5 Percentage of ephemeral ponds
Hindu Kush	Sparse (0.29-0.41/ km^2)	Remained low	Decreased during ablation season	Stable	85.3%
Karakoram		Showed a statistically significant increase (p-value < 0.05)		Increasing pond change events from 2017 to 2022	95.7% (highest in all sites)
Western Himalaya			Pond number decreased from July to October, pond area remained relatively stable		85.1%
Central Himalaya	Dense (0.68-1.5/ km^2)	Notable increase (44% from 2017 to 2020)	Pond number and area peaked in May or June and then declined during monsoon	Pond appearance, expansion, and merging events peaked in May/June then declined towards winter	82.8%
Eastern Himalaya		Notable increase (57% from 2018 to 2021)	Distinct seasonal change without a prominent and reliable seasonal cycle		87.3%

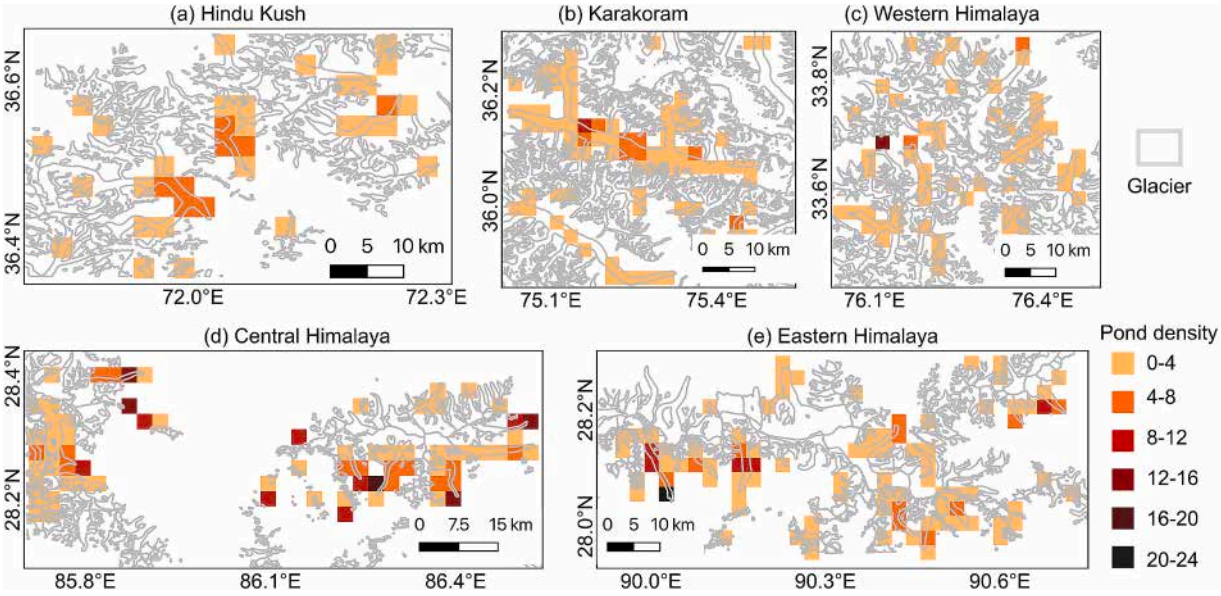

Fig. 4. Maps of supraglacial pond densities expressed as count divided by glacier area (units: number per km^2), shown in 0.025° ×0.025° grids, using October 2022 as a reference for comparison.

Table 5
The pond numbers and percentage of debris-covered area in October 2022.

Study site	Pond number	% of debris-covered area	Average pond density (number / km^2)
Hindu Kush	170	0.18	0.34
Karakoram	466	0.29	0.41
Western Himalaya	162	0.22	0.29
Central Himalaya	396	1.49	1.5
Eastern Himalaya	502	2.13	0.68

October fluctuated, but there was no clear inter-annual trend across the five sites (Fig. 6). The percentage ponded area increased significantly (p-value < 0.05) in the Karakoram and the Western Himalaya, while it remained low ($< 0.2\%$) in the Hindu Kush. In addition, the percentage ponded area increased by 57% in the Eastern Himalaya from 2018 to 2021 and by 44% in the Central Himalaya from 2017 to 2020, respectively.

Supraglacial ponds exhibited approximately 20% seasonal variation in both number and percentage ponded area across all study sites but the Karakoram during the study period (Fig. 7). At the Hindu Kush and Karakoram sites, the pond number and area decreased during the ablation season in most years, except for 2018 and 2020 (Fig. 7a–b). Notably, at the Karakoram site, pond number reached 1131 and covered 0.83% of the debris-covered area in May 2022, which was 2.4 times higher than the average level (478, 0.36%) (Fig. 7b). However, observations for other years were unavailable in May (beginning of ablation season) due to substantial snow cover.

At the Western and Central Himalayan sites, pond number and area decreased during the monsoon season, with more complex seasonal variability observed in the Eastern Himalaya. In the Western Himalaya, the pond number halved from approximately 200 in the monsoon season (July) to about 100 in the post-monsoon period (October), but the percentage area over debris-covered glaciers remained relatively stable at 0.2% (Fig. 7c). At the Central Himalaya site, the pond number and the percentage ponded area exhibited peak values predominantly in the pre-monsoon season (May/June) (Fig. 7d), followed by a consistent decline throughout the monsoon season, reaching the lowest levels in December, except for 2020 when there was an increase between July and October.

At the Eastern Himalaya site, supraglacial ponds displayed distinct variability without a prominent and reliable seasonal cycle (Fig. 7e). In 2019, 2021 and 2022, the percentage ponded area increased from the pre-monsoon season, peaked during the monsoon or post-monsoon

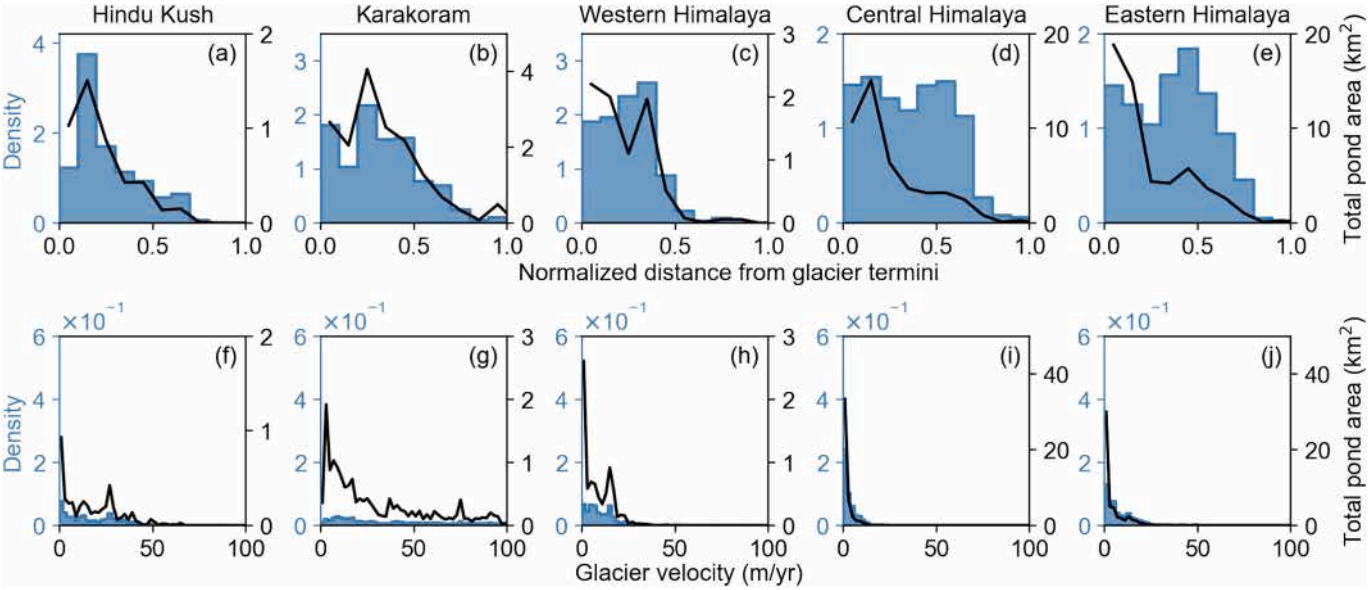

Fig. 5. Distribution of supraglacial ponds and glaciers with respect to (b) glacier velocity and (c) normalized distance from glacier termini. The black line indicates the sum of pond area in each bin.

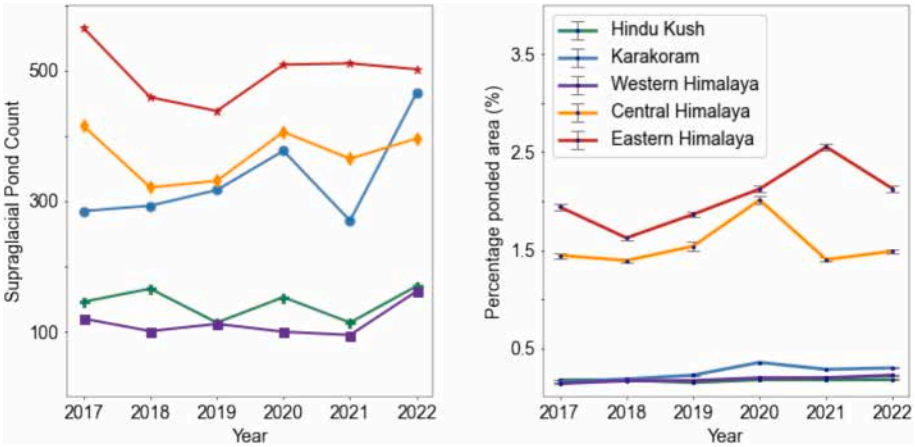

Fig. 6. (a) Time series of pond numbers at five selected sites (b) percentage ponded area over debris-covered area in October (lines with error bars). Note that the percentage areas were similar in the Western Himalaya and Hindu Kush.

period, and finally declined during the winter.

4.5. Dynamics of individual supraglacial ponds

4.5.1. Quantification of pond change events

The number of pond change events (group 1: appearance, disappearance, expansion; group 2: shrinkage, merging and splitting) exhibited regional differences across the five study sites (Fig. 8). The Hindu Kush site showed a relatively stable pattern of pond change events during the 2017-2022 period. In contrast, the Karakoram site experienced an increase in pond change events from 2017 to 2022. Notably, in May 2022, pond change events doubled compared to other Mays, with 952 pond appearances and 116 pond expansions; while from May to July, 719 ponds disappeared, and 243 ponds shrank. A similar but less pronounced pattern was observed in the Hindu Kush site, with more appearance and expansion events in May 2022 and more disappearance and shrinkage in July 2022 compared to other years.

Across the Himalayan sites, the supraglacial pond growth events (appearance, expansion, and merging) showed a consistent seasonal trend (Fig. 8c-e). The highest number of these events occurred during the pre-monsoon season, typically from May to June. Subsequently, the total number of pond appearance, expansion, and merging events declined during the monsoon season, reaching their lowest point in winter. In contrast, pond decrease events did not display an evident seasonal pattern. However, in the Eastern Himalaya, we observed a gradual increase in pond disappearance and shrinkage from the monsoon season to the post-monsoon (winter season) in 2021 and 2022.

4.5.2. Frequency of supraglacial ponds

The total number of unique supraglacial ponds, exhibited considerable variations across five study sites, ranging from 524 in the Western Himalaya to 2797 in the Karakoram (Table 6). The number of unique supraglacial ponds in the eastern and Central Himalaya is 2.6 to 3.5 times higher than that of the western sites except for the Karakoram site.

The quantification of pond frequency allows us to distinguish ephemeral, persistent, and permanent supraglacial ponds as shown in Fig. 9. Notably, at the Karakoram site, 95.7% of supraglacial ponds were identified as ephemeral ponds and 57.9% of supraglacial ponds there occurred only once or twice during the study period, with a frequency ranging from 0 to 0.1 (Fig. 10). The Central Himalaya had the highest

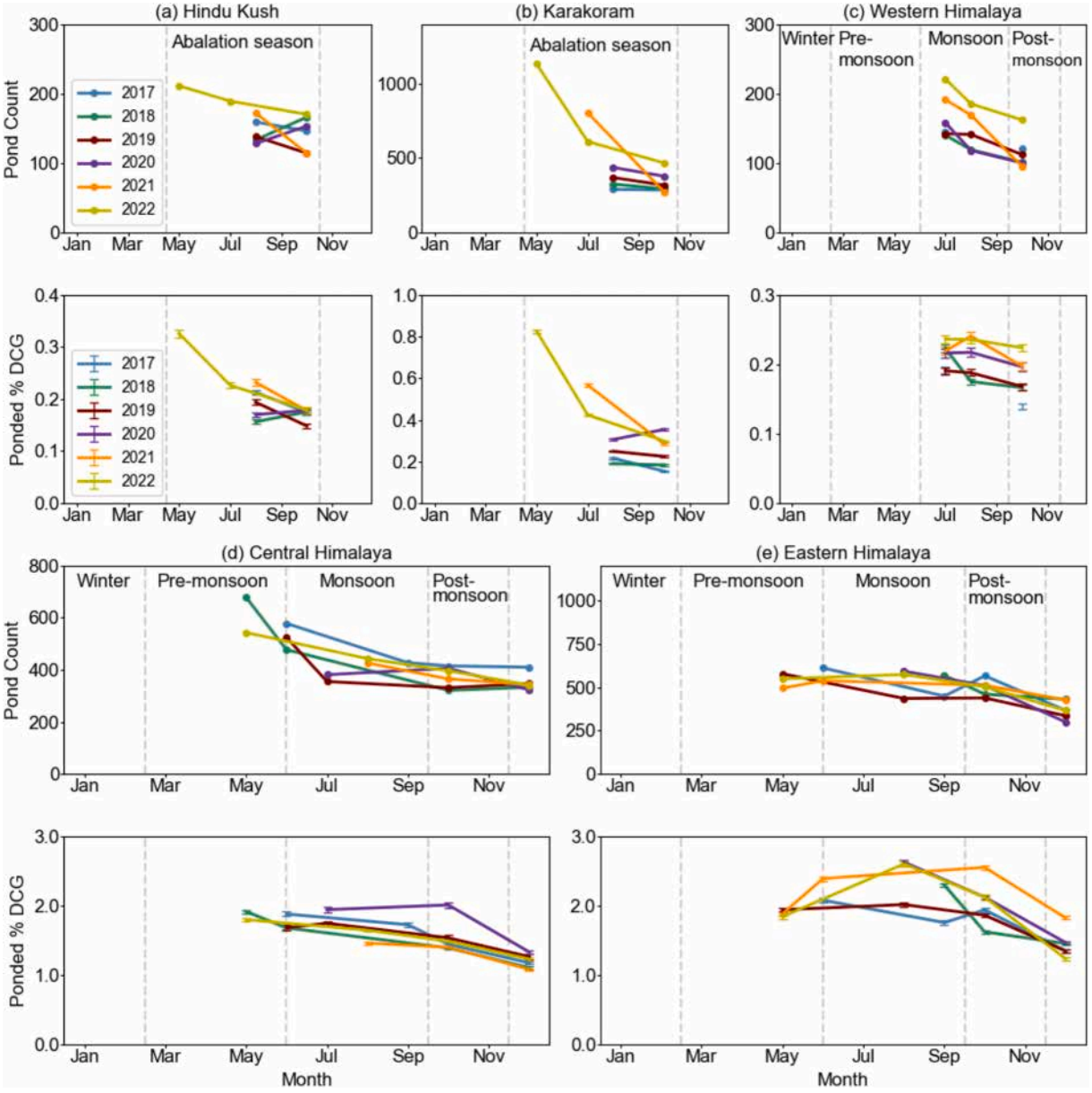

Fig. 7. Time series of pond numbers (vertical bars) and pond percentage area over debris cover from 2017 to 2022 at (a) Hindu Kush, (b) Karakoram, (c) Western Himalaya, (d) Central Himalaya, and (e) Eastern Himalaya.

proportion of persistent ponds (17.2%) and highest number of permanent ponds (43) throughout the entire period.

Approximately 96% of ephemeral supraglacial ponds were smaller than 0.01 km^2 (Fig. S13), while only 57% of persistent ponds were small-sized (<0.01 km^2). However, we observed no significant differences in their elevations and glacier settings (velocities and glacier sections) between ephemeral and persistent supraglacial ponds (Fig. S14).

5. Discussion

5.1. Advantages and limitations of the current data and method

Our deep-learning-based method enabled automated mapping of supraglacial ponds from multi-temporal PlanetScope images. This automated approach eliminates the need to determine thresholds for parameters like NDWI (Otsu, 1979; Huggel et al., 2002; Li and Sheng, 2012; Taylor et al., 2021), significantly improving the mapping efficiency from months to days for generating seasonal pond maps across the study sites from 2017 to 2022, compared to conventional manual and semi-automatic methods. Previous deep-learning-based mapping efforts for supraglacial ponds have been relatively limited, with one notable trial in Antarctica (Dirscherl et al., 2021). This limitation is particularly evident within the HKH ranges due to the complex topography and debris cover (Yuan et al., 2020). While there has been one attempt to use deep learning techniques for mapping supraglacial ponds in the Everest region using GaoFen-3 SAR images and a U-Net-based model (Chen, 2021), it faced difficulties in extracting small and narrow supraglacial ponds.

We improved the accuracy of supraglacial pond mapping in the HKH mountain ranges through three key aspects: the model, input satellite imagery, and training dataset. Firstly, we adopted DeepLabv3+ model, incorporating 'atrous' separable convolution to capture multi-scale contextual information, surpassing the other commonly used U-Net. Secondly, the use of high-resolution PlanetScope images (3.7 m) allowed for more precise pond boundaries than those obtained in previous studies using Landsat (30 m) and Sentinel-2 (10 m) imagery. Another

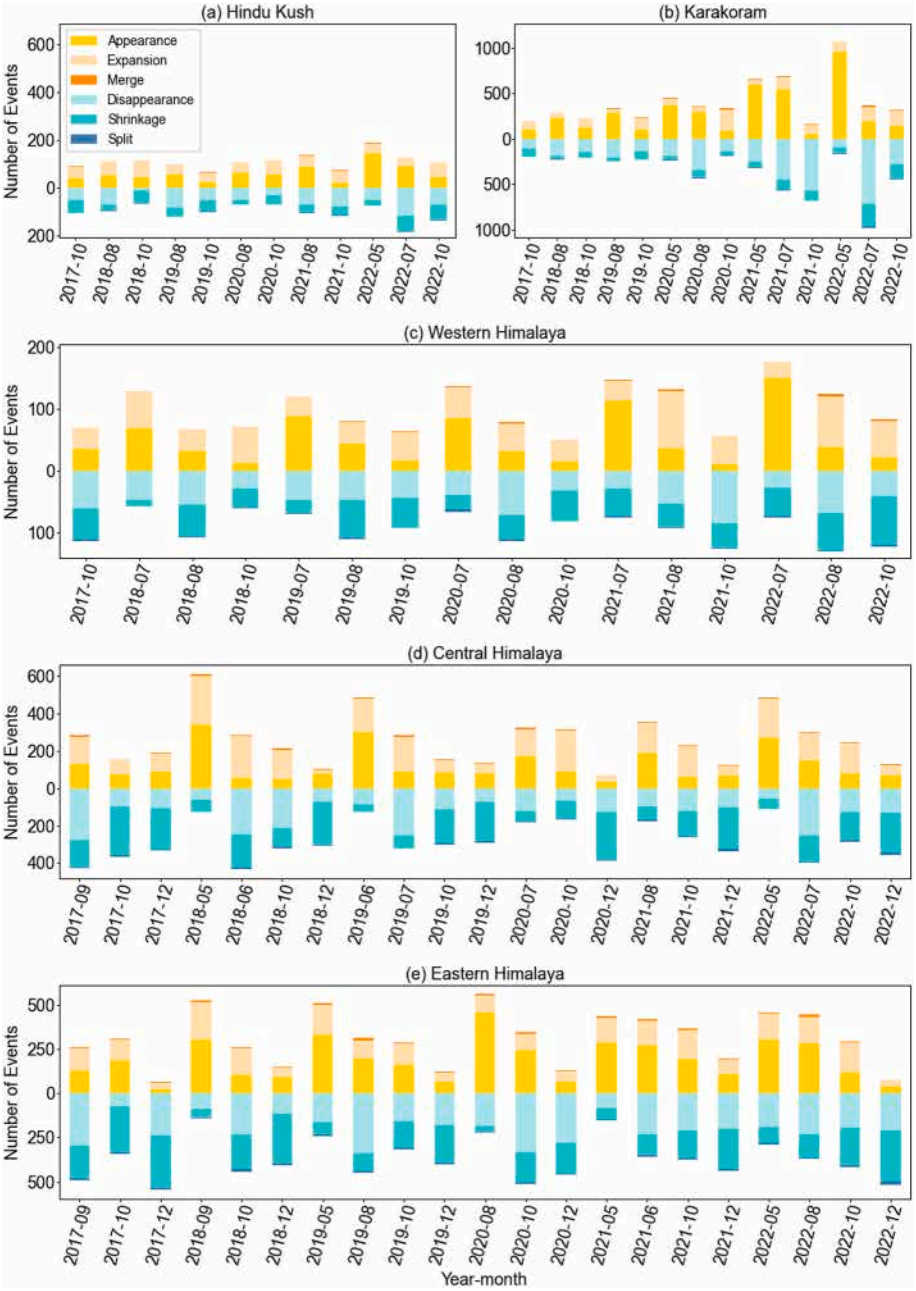

Fig. 8. Temporal changes in the numbers of appearances, expansion, merging, disappearance, shrinkage, and splitting events at five study sites.

Table 6
Numbers and percentages (in parenthesis) of different types of supraglacial ponds.

Study site	Unique ponds	Permanent ponds	Persistent ponds	Ephemeral ponds
Hindu Kush	538	5	79 (14.7%)	459 (85.3%)
Karakoram	2797	4	120 (4.3%)	2677 (95.7%)
Western Himalaya	524	11	78 (14.9%)	446 (85.1%)
Central Himalaya	1399	43	241 (17.2%)	1158 (82.8%)
Eastern Himalaya	1836	15	233 (12.7%)	1603 (87.3%)

strength of our mapping method is its combination of RGB and NDWI outputs, which helped identify ponds partially frozen or covered by cloud (Fig. 3f&3h). Furthermore, we used representative and diverse training samples, making our method applicable for extracting supraglacial ponds with various sizes, shapes, colors, textures, and context. Our approach enhanced the mapping accuracy and generalization of the mapping method compared to existing pond mapping methods such as threshold segmentation and U-Net based deep learning models. Because it was trained on diverse samples collected from the HKH regions, our model is well-suited for mapping ponds in regions with complex topography and pond characteristics.

Our mapping approach still has several limitations. First, we set a conservative area threshold for the mapped supraglacial ponds (0.0005 km^2) according to the image resolution to ensure reliable identification and differentiation of these ponds from other features such as snow slushes and shadows from ice cliff in the PlanetScope imagery. Assuming

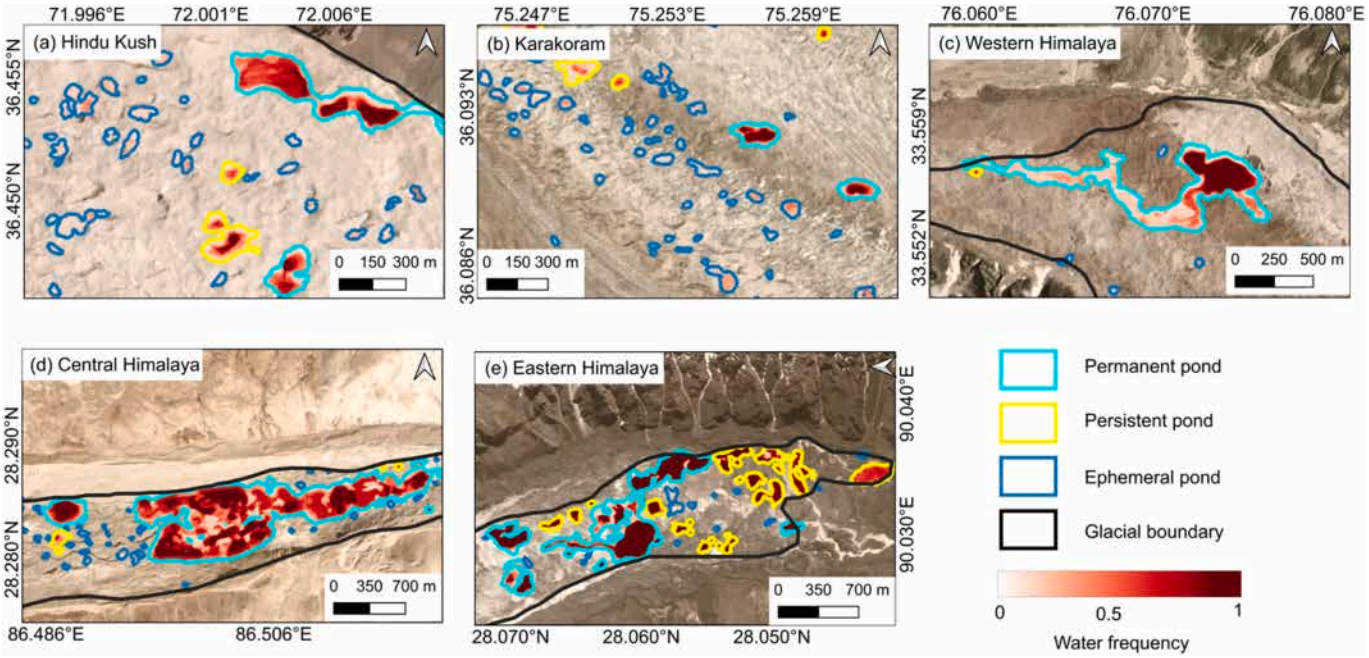

Fig. 9. Examples of permanent, persistent, and ephemeral ponds at each of the five study sites.

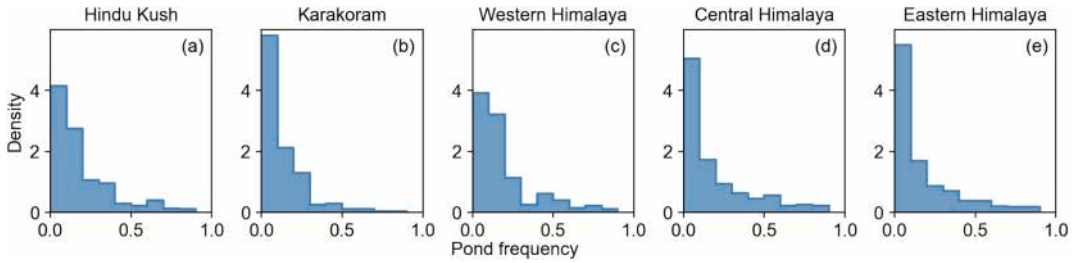

Fig. 10. Statistical distribution of supraglacial pond frequency.

our pond size-frequency distribution follows the log-linear fit relationship (Miles et al., 2017b), the exclusion of ponds smaller than 0.0005 km^2 (Fig. S15) would result in approximately 17.9% of the total pond area being omitted. However, incorporating smaller ponds would compromise the dataset reliability due to the reduced ability to accurately identify small, turbid, and brown-surfaced supraglacial ponds (Fig. S16a&b).

Furthermore, we adopted the RGI 7.0 glacier outlines to separate supraglacial ponds from water bodies within glacier boundaries. The accuracy and reliability of our supraglacial pond maps are therefore influenced by the glacier boundaries adopted, particularly as many supraglacial ponds are clustered near the glacier termini. Any temporal changes or boundary errors in glacier termini may have an impact on the resulting pond maps as well as subsequent analyses related to pond number and area. We acknowledge that RGI 7.0 glacier outlines (corresponding to ~year 2000) (RGI 7.0 Consortium, 2023) do not fully represent the glacier boundaries during our study period (2017–2022), necessitating the post-processing to refining pond compilation.

Additionally, there is an inconsistency between our pond datasets and the debris cover datasets utilized. The debris cover boundaries in Scherler et al. (2018a) were derived from Landsat-8 and Sentinel-2 satellite images from the period 2013-2017, and we assumed a constant extent throughout our study period (2017-2022). Considering that the supraglacial debris cover expanded up-glacier due to negative mass balance (Jiang et al., 2018; Compagno et al., 2022), we visually inspected and corrected misclassed or missed supraglacial ponds. This approach ensured a more comprehensive pond assessment.

Moreover, the model performance decreased for frozen or snow-covered supraglacial ponds (Fig. S16c), which are challenging to identify. This can be attributed to factors such as a lack of discriminative features, reduced contrast and texture, similarity to surrounding snow or glaciers, and limited training samples. Zeller et al. (2024) has contributed to pond mapping during winter which required accurate ice identification and comparison with prior water mask to determine frozen lake. Further efforts are warranted to address the challenges posed by winter conditions and enhance the identification of frozen or snow-covered supraglacial ponds.

Further developments should focus on employing high-performing deep learning networks to achieve higher mapping accuracy for supraglacial ponds with complex shapes, frozen surface, or those inside landmass. From a methodological perspective, it would be beneficial to adopt a network that can accommodate four or more bands, thereby allowing to incorporate additional spectral or terrain information. Moreover, specialized algorithms or models specifically trained for winter pond detection could be developed. From a data perspective, the inclusion of SAR images should be considered to supplement optical images for pond mapping, as radar signals can penetrate clouds and shallow snow and ice on the water surface (Wangchuk and Bolch, 2020; Chen, 2021). For instance, as shown in Fig. S17, supraglacial ponds in our Central Himalaya study site can be distinguished from SAR images even when they are still frozen and indistinguishable in optical images.

5.2. Contrasting distribution patterns of supraglacial ponds across the HKH

Our findings revealed a distinct east-west gradient in the distribution of supraglacial ponds across the HKH mountain ranges, consistent with the findings from Gardelle et al. (2011). The contrasting pond distribution is likely influenced by the regionally-varying glacier mass balance, monsoon precipitation, and topographic settings (Scherler et al., 2011; Sakai and Fujita, 2010). Specifically, higher pond cover and dense distribution observed in the Central and Eastern Himalaya can be attributed to significant negative glacier mass balance (King et al., 2017; Shean et al., 2020), higher monsoon precipitation (Racoviteanu et al., 2021) and the presence of low-slope, low-velocity, debris-covered glacier tongues (Dehecq et al., 2015; Thompson et al., 2016; Watson et al., 2016). Glacier mass loss and rainfall supply abundant water, while the low-gradient, near-stagnant glacier tongues allow the glacial meltwater and precipitation to accumulate in surface depressions, facilitating formation and expansion of supraglacial ponds (Reynolds, 2000; Miles et al., 2017b; Taylor et al., 2021). The Indian summer monsoon precipitations in June-July-August (JJA) showed large differences between the Central and Eastern Himalaya and the other three areas in the western part of the HKH (Fig. 11b). The JJA rainfall in the Central and Eastern Himalaya exceeded 600 mm every year whereas the precipitation was below 400 mm in the Hindu Kush, Karakoram, and Western Himalaya.

Supraglacial ponds in the Central and Eastern Himalaya were concentrated in areas with glacier velocities below 20 m/yr, higher than the velocities (below 8 m/yr) reported by Taylor et al. (2021). Notably, over 40% of supraglacial ponds were located in the middle to upper sections of glaciers in these two sites, contrasting with other sites and previous observations that ponds are concentrated near glacier termini (Zeller et al., 2024).

Fewer supraglacial ponds were sparsely distributed at the Western Himalaya and the Hindu Kush sites. These regions receive less meltwater and precipitation input for the formation of supraglacial ponds compared to the Central and Eastern Himalaya. We also observed low pond coverage in the Karakoram with 42% of the ponds smaller than $<0.001\ km^2$ (Fig. S9). However, the number of supraglacial ponds in the Karakoram was comparable to those in the Central and Eastern Himalaya, possibly due to the glacier melting and thin debris cover (0-0.5 m) (Fig. S19). Glaciers in the Karakoram exhibited accelerated thinning in the late 2010s (Hugonnet et al., 2021), providing meltwater for pond formation. The thin supraglacial debris layer enhances surface melting by absorbing more solar radiation compared to clean ice, promoting the formation of supraglacial ponds (Rounce et al., 2021; Chen et al., 2023). We acknowledge that the debris thickness dataset (Rounce et al., 2021) used in this study was derived from a model based on satellite brightness temperature measurements, bearing significant uncertainty, particularly in areas containing supraglacial ponds.

Factors such as slope, longitudinal gradient, and englacial connectivity can influence the distribution of supraglacial ponds. However, we did not investigate nor compared the pond distribution with respect to these conditions due to the unavailability of high-quality and consistent datasets across the HKH ranges.

5.3. Interannual variabilities and seasonality of supraglacial ponds across the HKH

Supraglacial ponds demonstrated contrasting interannual variabilities in pond area during our study period (2017-2022), with stable pond cover in the Hindu Kush and increases in other sites. The increase of supraglacial ponds in the Central and Eastern Himalaya and the consistently low pond area in the Hindu Kush align with the trends reported by Gardelle et al. (2011) from 1990 to 2009 and Nie et al. (2017)

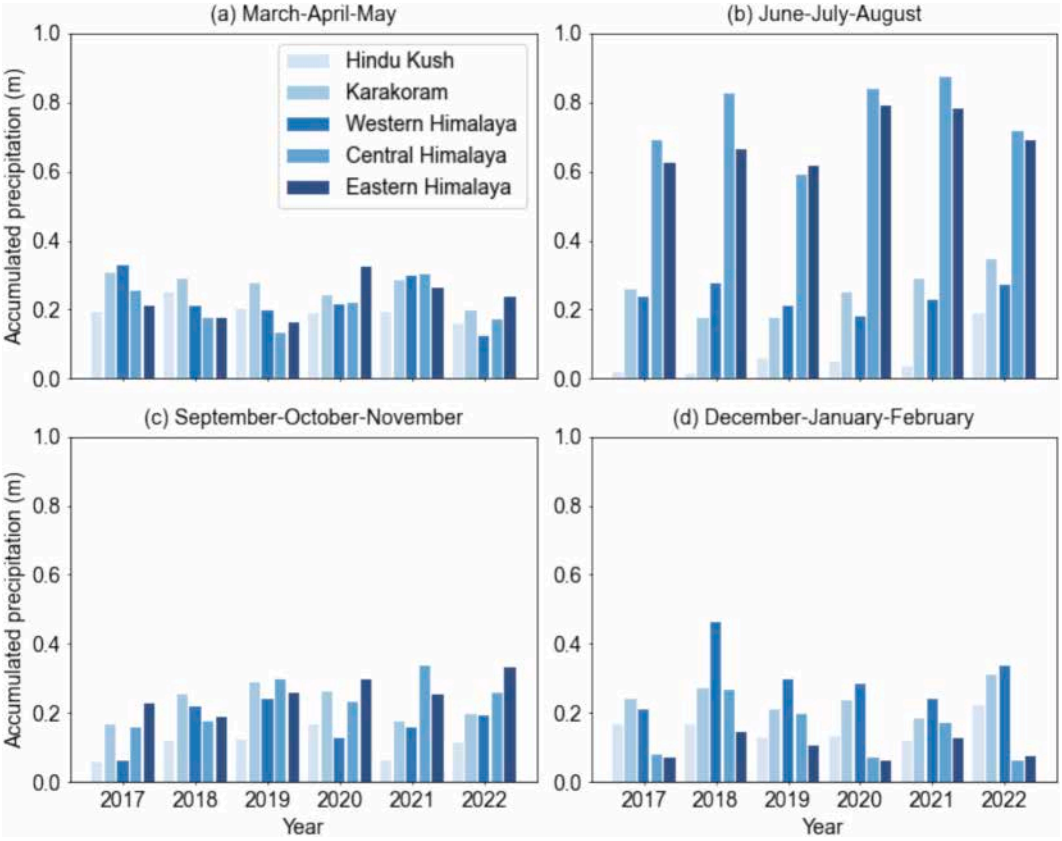

Fig. 11. (a) March-April-May (MAM) precipitation, (b) June-July-August (JJA) precipitation, (c) September-October-November (SON) precipitation, and (d) December-January-February (DJF) precipitation from ERA5-Land hourly climate reanalysis dataset at five selected sites.

between 1990 and 2015. In the Eastern Himalaya, we noted a moderate correlation between the change of the pond percentage area with the Indian summer monsoon precipitations (June to August), as shown in Fig. 11b. The percentage ponded area had been exhibiting significant increases in the Eastern Himalaya from 2018 until a drop in 2022, similar to the trend in the summer monsoon precipitation, rising from 2019 to 2021 and declining in 2022.

At the Karakoram site, we observed a gradual increase in pond area from 2017 to 2020, consistent with the findings of Wendleder et al. (2021), who reported a linear increase in the pond area at a rate of 11.12% per year on the Baltoro glacier in the Karakoram between 2016 and 2020. This, however, is in contrast with the reported decreasing trend (~-0.4 ha/year) between 1990 and 2009 in Gardelle et al., 2011. This discrepancy highlights the unique glaciological behavior of the Karakoram region compared to the rest of the HKH. This region is characterized by glacier stability or slight mass gain since 2000 (Hewitt, 2005; Hewitt, 2014), referred to as the Karakoram anomaly, which is slowly coming to an end as suggested by recent studies (Hugonnet et al., 2021; Bhattacharya et al., 2021; Yao et al., 2022; Jackson et al., 2023). The shift from a decrease to a slight increase in pond area in the Karakoram may be indicative of the diminishing glacier anomaly in this region (Hugonnet et al., 2021). Moreover, simultaneous increases in the pond area and summer rainfall were observed in the Karakoram (Fig. 11b).

The seasonal variability of supraglacial ponds in number and area amounted to ~ 20% across five sites except for Karakoram reaching 52% mainly due to the anomaly in 2022. In May 2022, the Karakoram sites recorded a peak number of 1131 supraglacial ponds, exceeding the average level by over twofold (478). A total of 952 supraglacial ponds formed before May, and 719 supraglacial ponds completely drained before July. The comparison of PlanetScope-based observations in late May between 2022 and previous years (Fig. S18) suggests an earlier onset of melting in 2022. In previous years, the glaciers remained frozen until late May. The accelerated glacier ice melt contribute to the formation of numerous supraglacial ponds on glacier surface.

In the monsoon-influenced sites of the Western and Central Himalaya, supraglacial ponds decreased from pre-monsoon or monsoon season to winter for most years. The Western Himalaya study site is situated in a transitional region influenced by both the westerlies to Indian Summer monsoon, where the long-lasting snow cover from November to the following June limits the observations in the winter and pre-monsoon seasons. However, in the Eastern Himalaya, the patterns of pond seasonal variation were more complex and diverse. The pond area increased from pre-monsoon and reached its peak during monsoon or post-monsoon season in 2019, 2021 and 2022. Our observations indicated that the seasonal changes of the supraglacial pond area in Eastern Himalaya sites showed consistency with the seasonal temperature and total precipitation (Fig. 12b). Numerous supraglacial ponds thawed and appeared starting from around May, with the peak appearance occurring in the pre-monsoon season (Fig. 9), possibly due to increased meltwater availability when ablation started. Substantial precipitation during the monsoon sustained high levels of pond appearance and expansion (Fig. 9). The decrease in pond area from monsoon to post-monsoon season in most years could be attributed to frequent pond drainage events, where more supply of meltwater or precipitation facilitates pond drainage into englacial networks via opening conduits (Taylor et al., 2021). Subsequently, the number and area of supraglacial ponds declined in the winter due to drainage and freezing. The influence of glacier settings such as the seasonal changes in mass balance and ice velocities as well as englacial networks should also be considered but not discussed here due to the lack of high-resolution and field datasets.

The seasonal pattern observed in the Eastern Himalaya aligns with the findings reported by Miles et al. (2017b) for supraglacial ponds over five glaciers in the Langtang Valley, Nepal. Their study documented pond emergence during pre-monsoon, peaking at monsoon onset at 2% of debris-covered area, and declining post-monsoon. Similarly, Chand and Watanabe (2019) highlighted pronounced seasonal variability for ponds on 23 debris-covered glaciers in the Everest region from 1989 to 2017. Their findings revealed comparably high pond area being during the pre- and post-monsoon seasons and lowest in the winter. Zeller et al. (2024) documented a slightly different pattern of pond changes in eight

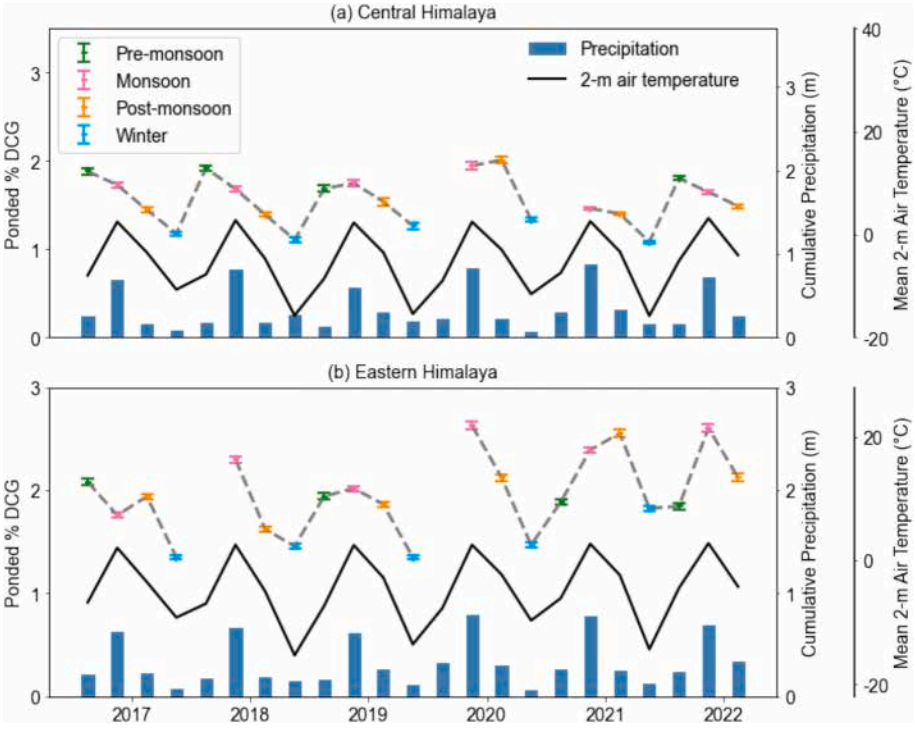

Fig. 12. Time series of pond area percentage over debris cover (dashed lines with error bars), seasonally cumulative precipitation (vertical bars) and seasonal mean 2-m air temperature (T2m) (thick black lines) in the (a) Central Himalaya and (b) Eastern Himalaya.

glaciers in the Khumbu region, Nepal, where pond area reached its peak in March, decreased during the monsoon season to its minimum in September, and then demonstrated a steady increase through post-monsoon and winter periods based on daily Planet observations. Due to the data gaps and seasonal interval of generated maps, we are unable to capture the winter increase and daily pond variation. The adequate characterization and comparison of pond seasonality with Zeller et al. (2024) required higher-frequency and long-term observations. Our findings also allow for the quantification of individual-pond-scale changes as well as glacier-wide assessments of pond dynamics. Our study specifically focuses on the local scale analysis to characterize the condition of ponds and highlight regional contrasts.

5.4. Pond persistency variations and associated influencing factors across the HKH

The climate conditions and glacial environments, characterized by factors such as debris thickness, glacier velocity, glacier mass loss, and englacial connectivity, play vital roles in determining the dynamics and lifespan of supraglacial ponds across the study sites. Ephemeral supraglacial ponds accounted for approximately 85% of the total at most study sites, with the Karakoram exhibiting a much higher proportion (95.7%), indicating their highly dynamic and transient nature. The frequent formation and drainage of ponds in the Karakoram could be attributed to the thin debris layer (0-0.5 m) covering the glacier surface and the high glacier velocity of up to 100 m/yr there (Fig. S19 &S20). While the thin debris enhanced surface melting and pond formation (Rounce et al., 2021; Chen et al., 2023), the rapid ice flow enhances the connectivity between the supraglacial and englacial hydrologic systems, facilitating pond drainage and hindering the expansion or persistence of supraglacial ponds (Miles et al., 2017b).

On the contrary, the Central and Eastern Himalayan sites exhibit a higher prevalence of persistent supraglacial ponds compared to other sites. Several factors contribute to the persistence of these supraglacial ponds. Firstly, the abundant glacier melting water and substantial monsoon precipitation supply the consistent water input, supporting the formation and longevity of supraglacial ponds. In addition, the relatively low glacier velocity of the debris cover part provides a stable environment for water accumulation in the supraglacial environment. Furthermore, small supraglacial ponds can coalescence and have the potential to transform into large terminal glacial lakes. This process involves the accumulation of large volume of water, reducing the likelihood of complete drainage of ponds through englacial channels.

Within each study site, our results reveal that there was no significant difference in the topographic and glacier settings between persistent and ephemeral supraglacial ponds (Fig. S13). Both types of supraglacial ponds were distributed within similar elevation ranges, glacier velocity ranges, and sections of glaciers. These findings indicate that the persistence of supraglacial ponds at a local scale is likely controlled by factors associated with the connectivity to englacial networks within the glaciers. Further investigations, including field observations, are warranted to explore the specific mechanisms behind englacial processes that govern the persistence or transience of supraglacial ponds.

6. Conclusions and perspectives

In this paper we successfully applied an advanced deep-learning-based method for mapping supraglacial ponds and investigated their spatio-temporal variability. We automatically mapped supraglacial ponds at five sites across the HKH from 2017 to 2022 at seasonal scales. The results demonstrated the applicability and transferability of our approach in mapping supraglacial ponds from multi-temporal satellite images, and enabled us to efficiently produce high-quality supraglacial pond datasets with an error (1.41 pixels) comparable to human level for analyzing their spatial-temporal variations.

This study provides a first representative overview of spatial-temporal variation of supraglacial ponds in the HKH range, revealing significant regional differences in pond distribution, interannual changes, seasonal variations, and persistency. Specifically, we found that

(1) the mean percentage ponded area over the debris-covered area in the Central Himalaya (1.55%) and Eastern Himalaya (1.93%) were significantly higher compared to the sites in the Hindu Kush (0.19%), Karakoram (0.36%), and Western Himalaya (0.20%), which was attributed to substantial glacier mass loss and abundant monsoon precipitation in the eastern HKH;
(2) pond total area increased from 2017 to 2022 except in the Hindu Kush, which remained consistently low ($< 0.2\%$);
(3) supraglacial ponds generally decreased during the ablation/monsoon season, except in the Eastern Himalaya, where peak pond area was observed during monsoon or post-monsoon periods;
(4) the Karakoram exhibited the highest proportion of ephemeral ponds (95.7%), while the Central and Eastern Himalaya contained more persistent supraglacial ponds.

We found regional heterogeneity of pond distribution and evolution at local scales and seasonal intervals. The controlling factors on pond spatial-temporal changes across different regions required further investigation with more comprehensive datasets on glacier dynamics and local hydrological systems.

Understanding the dynamics of supraglacial ponds is crucial for comprehending the broader implications for glacial meltwater storage, runoff patterns, and the overall mass balance of glaciers. Further research is needed to investigate the complex interactions between debris cover, glacier velocity, englacial connectivity, and the behavior of supraglacial ponds across diverse glacial environments. This knowledge holds the potential to enhance predictions of glacial response to climate change and shed light on its downstream water resources impact.

CRediT authorship contribution statement

Xingyu Xu: Writing – original draft, Methodology, Investigation. **Lin Liu:** Writing – review & editing, Supervision, Conceptualization. **Lingcao Huang:** Validation, Methodology. **Yan Hu:** Writing – review & editing, Validation. **Guoqing Zhang:** Writing – review & editing, Supervision. **Adina Racoviteanu:** Methodology, Writing – review & editing. **Emily Victoria Liu:** Data curation. **YingTo Agnes Chan:** Data curation.

Declaration of competing interest

The authors declare that they have no known competing financial interests or personal relationships that could have appeared to influence the work reported in this paper.

Acknowledgement

Great thanks to Professor Stephan Harrison for providing guidance and insights. This work is supported by the following research grants: the Hong Kong Research Grants Council (HKPFS PF18-21555, CUHK14303119, CUHK14302421, F-CUHK404/22)) and the CUHK Direct Grant for Research (4053592 and 4053644). Adina Racoviteanu's contribution was supported by the French National Research Institute for Sustainable Development (IRD) and the PROCORE FRANCE- HONG KONG project 49478PK.

Appendix A. Supplementary data

Supplementary data to this article can be found online at https://doi.

org/10.1016/j.gloplacha.2025.104949.

Data availability

The PlanetScope CubeSat images are copyrighted by Planet Labs Inc., restricted by commercial policies and are not open to the public. The supraglacial pond inventories are accessible through Xu et al., (2023), Zenodo, https://doi.org/10.5281/zenodo.7984795

References

Azam, M.F., Wagnon, P., Berthier, E., Vincent, C., Fujita, K., Kargel, J.S., 2018. Review of the status and mass changes of Himalayan-Karakoram glaciers. J. Glaciol. 64 (243), 61–74.

Benn, D.I., Wiseman, S., Warren, C.R., 2000. Rapid growth of a supraglacial lake, Ngozumpa Glacier, Khumbu Himal, Nepal. In: Debris-Covered Glaciers. International Association of Hydrological Sciences, pp. 177–185.

Benn, D.I., Wiseman, S., Hands, K.A., 2001. Growth and drainage of supraglacial lakes on debris-mantled Ngozumpa Glacier, Khumbu Himal, Nepal. J. Glaciol. 47 (159), 626–638.

Benn, D.I., Bolch, T., Hands, K., Gulley, J., Luckman, A., Nicholson, L.I., Quincey, D., Thompson, S., Toumi, R., Wiseman, S., 2012. Response of debris-covered glaciers in the Mount Everest region to recent warming, and implications for outburst flood hazards. Earth Sci. Rev. 114 (1–2), 156–174.

Bhattacharya, A., Bolch, T., Mukherjee, K., King, O., Menounos, B., Kapitsa, V., Yao, T., 2021. High Mountain Asian glacier response to climate revealed by multi-temporal satellite observations since the 1960s. Nat. Commun. 12 (1), 4133.

Bolch, T., Buchroithner, M.F., Peters, J., Baessler, M., Bajracharya, S., 2008. Identification of glacier motion and potentially dangerous glacial lakes in the Mt. Everest region/Nepal using spaceborne imagery. Nat. Hazards Earth Syst. Sci. 8 (6), 1329–1340.

Bookhagen, B., Burbank, D.W., 2006. Topography, relief, and TRMM-derived rainfall variations along the Himalaya. Geophys. Res. Lett. 33 (8).

Bookhagen, B., Thiede, R.C., Strecker, M.R., 2005. Late Quaternary intensified monsoon phases control landscape evolution in the northwest Himalaya. Geology 33 (2), 149–152.

Casey, K.A., Kääb, A., Benn, D.I., 2012. Geochemical characterization of supraglacial debris via in situ and optical remote sensing methods: a case study in Khumbu Himalaya, Nepal. Cryosphere 6 (1), 85–100.

Chand, M.B., Watanabe, T., 2019. Development of supraglacial ponds in the Everest Region, Nepal, between 1989 and 2018. Remote Sens. 11 (9), 1058.

Chen, F., 2021. Comparing methods for segmenting supra-glacial lakes and surface features in the mount everest region of the himalayas using Chinese GaoFen-3 SAR images. Remote Sens. 13 (13), 2429.

Chen, L.C., Zhu, Y., Papandreou, G., Schroff, F., Adam, H., 2018. Encoder-decoder with atrous separable convolution for semantic image segmentation. In: Proceedings of the European Conference on Computer Vision (ECCV), pp. 801–818.

Chen, F., Zhang, M., Guo, H., Allen, S., Kargel, J.S., Haritashya, U.K., Watson, C.S., 2021. Annual 30 m dataset for glacial lakes in High Mountain Asia from 2008 to 2017. Earth Syst. Sci. Data 13 (2), 741–766.

Chen, F., Wang, J., Li, B., Yang, A., Zhang, M., 2023. Spatial variability in melting on Himalayan debris-covered glaciers from 2000 to 2013. Remote Sens. Environ. 291, 113560.

Compagno, L., Huss, M., Miles, E.S., McCarthy, M.J., Zekollari, H., Dehecq, A., Farinotti, D., 2022. Modelling supraglacial debris-cover evolution from the single-glacier to the regional scale: an application to High Mountain Asia. Cryosphere 16 (5), 1697–1718.

Dehecq, A., Gourmelen, N., Trouve, E., 2015. Deriving large-scale glacier velocities from a complete satellite archive: application to the Pamir–Karakoram–Himalaya. Remote Sens. Environ. 162, 55–66.

Dirscherl, M., Dietz, A.J., Kneisel, C., Kuenzer, C., 2021. A novel method for automated supraglacial lake mapping in Antarctica using Sentinel-1 SAR imagery and deep learning. Remote Sens. 13 (2), 197.

Dyurgerov, M.B., Meier, M.F., 2005. Glaciers and the changing Earth system: a 2004 snapshot, 58. Institute of Arctic and Alpine Research, University of Colorado, Boulder, p. 23.

European Space Agency, 2024. Copernicus Global Digital Elevation Model GLO-30. Available at. https://doi.org/10.5270/ESA-c5d3d65).

Gardelle, J., Arnaud, Y., Berthier, E., 2011. Contrasted evolution of glacial lakes along the Hindu Kush Himalaya mountain range between 1990 and 2009. Glob. Planet. Chang. 75 (1-2), 47–55.

Gardner, A.S., Fahnestock, M.A., Scambos, T.A., 2019. ITS_LIVE Regional Glacier and Ice Sheet Surface Velocities. National Snow and Ice Data Center.

Hewitt, K., 2005. The Karakoram anomaly? Glacier expansion and the'elevation effect, 'Karakoram Himalaya'. Mt. Res. Dev. 332–340.

Hewitt, K., 2014. Glaciers of the Karakoram Himalaya. In: Singh, V.P., Singh, P., Haritashya, U.K. (Eds.), Encyclopedia of Snow, Ice and Glaciers. Springer, Netherlands, Dordrecht, pp. 429–436.

Hochreuther, P., Neckel, N., Reimann, N., Humbert, A., Braun, M., 2021. Fully automated detection of supraglacial lake area for Northeast Greenland using Sentinel-2 time-series. Remote Sens. 13 (2), 205.

Huang, L., Luo, J., Lin, Z., Niu, F., Liu, L., 2020. Using deep learning to map retrogressive thaw slumps in the Beiluhe region (Tibetan Plateau) from CubeSat images. Remote Sens. Environ. 237, 111534.

Huang, L., Lantz, T.C., Fraser, R.H., Tiampo, K.F., Willis, M.J., Schaefer, K., 2022. Accuracy, efficiency, and transferability of a deep learning model for mapping retrogressive thaw slumps across the Canadian Arctic. Remote Sens. 14 (12), 2747.

Huggel, C., Kääb, A., Haeberli, W., Teysseire, P., Paul, F., 2002. Remote sensing based assessment of hazards from glacier lake outbursts: a case study in the swiss alps. Canadian Geotechnical Journal 39 (2), 316–330.

Hugonnet, R., McNabb, R., Berthier, E., Menounos, B., Nuth, C., Girod, L., Farinotti, D., Huss, M., Dussaillant, I., Brun, F., Kääb, A., 2021. Accelerated global glacier mass loss in the early twenty-first century. Nature 592, 726–731.

Irvine-Fynn, T.D.L., Porter, P.R., Rowan, A.V., Quincey, D.J., Gibson, M.J., Bridge, J.W., Watson, C.S., Hubbard, A., Glasser, N.F., 2017. Supraglacial ponds regulate runoff from Himalayan debris-covered glaciers. Geophys. Res. Lett. 44, 11894–11904.

Jackson, M., Azam, M.F., Baral, P., Benestad, R., Brun, F., Muhammad, S., Thapa, A., 2023. Consequences of climate change for the cryosphere in the Hindu Kush Himalaya. In: Wester, P., Chaudhary, S., Chettri, N., Jackson, M., Maharjan, A., Nepal, S., Steiner, J.F. (Eds.), Water, ice, society, and ecosystems in the Hindu Kush Himalaya: An outlook ICIMOD. International Centre for Integrated Mountain Development (ICIMOD), Kathmandu, Nepal, pp. 17–71.

Jiang, S., Nie, Y., Liu, Q., Wang, J., Liu, L., Hassan, J., Xu, X., 2018. Glacier change, supraglacial debris expansion and glacial lake evolution in the Gyirong river basin, central Himalayas, between 1988 and 2015. Remote Sens. 10 (7), 986.

Johansson, A.M., Brown, I.A., 2013. Adaptive classification of supra-glacial lakes on the West Greenland Ice Sheet. IEEE J. Sel. Top. Appl. Earth Obs. Remote Sens. 6 (4), 1998–2007.

Kääb, A., Berthier, E., Nuth, C., Gardelle, J., Arnaud, Y., 2012. Contrasting patterns of early twenty-first-century glacier mass change in the Himalayas. Nature 488, 495–498.

Khadka, N., Zhang, G., Thakuri, S., 2018. Glacial lakes in the Nepal Himalaya: Inventory and decadal dynamics (1977–2017). Remote Sens. 10 (12), 1913.

King, O., Quincey, D.J., Carrivick, J.L., Rowan, A.V., 2017. Spatial variability in mass loss of glaciers in the Everest region, central Himalayas, between 2000 and 2015. Cryosphere 11 (1), 407–426.

King, O., Bhattacharya, A.A., Bhambri, R., Bolch, T., 2019. Glacial lakes exacerbate Himalayan glacier mass loss. Sci. Report. 9, 18145.

Kneib, M., Miles, E.S., Buri, P., Molnar, P., McCarthy, M., Fugger, S., Pellicciotti, F., 2021a. Interannual dynamics of ice cliff populations on debris-covered glaciers from remote sensing observations and stochastic modeling. J. Geophys. Res. Earth Surf. 126 (10), e2021JF006179.

Kneib, M., Miles, E.S., Jola, S., Buri, P., Herreid, S., Bhattacharya, A., Pellicciotti, F., 2021b. Mapping ice cliffs on debris-covered glaciers using multispectral satellite images. Remote Sens. Environ. 253, 112201.

Kraaijenbrink, P.D.A., Shea, J.M., Pellicciotti, F., De Jong, S.M., Immerzeel, W.W., 2016. Object-based analysis of unmanned aerial vehicle imagery to map and characterise surface features on a debris-covered glacier. Remote Sens. Environ. 186, 581–595.

Li, J., Sheng, Y., 2012. An automated scheme for glacial lake dynamics mapping using Landsat imagery and digital elevation models: a case study in the Himalayas. Int. J. Remote Sens. 33 (16), 5194–5213.

Lutz, K., Bahrami, Z., Braun, M., 2023. Supraglacial Lake Evolution over Northeast Greenland Using Deep Learning Methods. Remote Sens. 15 (17), 4360.

Maharjan, S.B., Mool, P.K., Lizong, W., Xiao, G., Shrestha, F., Shrestha, R.B., Khanal, N., Bajracharya, S., Joshi, S., Shahi, S., Baral, P., 2018. The Status of Glacial Lakes in the Hindu Kush Himalaya-ICIMOD Research Report 2018/1.

Mertes, J.R., Thompson, S.S., Booth, A.D., Gulley, J.D., Benn, D.I., 2017. A conceptual model of supra-glacial lake formation on debris-covered glaciers based on GPR facies analysis. Earth Surf. Process. Landf. 42 (6), 903–914.

Miles, E.S., Pellicciotti, F., Willis, I.C., Steiner, J.F., Buri, P., Arnold, N.S., 2016. Refined energy-balance modelling of a supraglacial pond, Langtang Khola, Nepal. Ann. Glaciol. 57 (71), 29–40.

Miles, E.S., Steiner, J., Willis, I., Buri, P., Immerzeel, W.W., Chesnokova, A., Pellicciotti, F., 2017a. Pond dynamics and supraglacial-englacial connectivity on debris-covered Lirung Glacier, Nepal. Front. Earth Sci. 5, 69.

Miles, E.S., Willis, I.C., Arnold, N.S., Steiner, J., Pellicciotti, F., 2017b. Spatial, seasonal and interannual variability of supraglacial ponds in the Langtang Valley of Nepal, 1999–2013. J. Glaciol. 63 (237), 88–105.

Miles, E.S., Willis, I., Buri, P., Steiner, J.F., Arnold, N.S., Pellicciotti, F., 2018. Surface pond energy absorption across four Himalayan glaciers accounts for 1/8 of total catchment ice loss. Geophys. Res. Lett. 45 (19), 10–464.

Mitkari, K.V., Arora, M.K., Tiwari, R.K., 2017. Extraction of glacial lakes in gangotri glacier using object-based image analysis. IEEE J. Sel. Top. Appl. Earth Obs. Remote Sens. 10 (12), 5275–5283.

Mölg, N., Ferguson, J., Bolch, T., Vieli, A., 2020. On the influence of debris cover on glacier morphology: How high-relief structures evolve from smooth surfaces. Geomorphology 357, 107092.

Muñoz-Sabater, J., Dutra, E., Agustí-Panareda, A., Albergel, C., Arduini, G., Balsamo, G., Thépaut, J.N., 2021. ERA5-Land: A state-of-the-art global reanalysis dataset for land applications. Earth Syst. Sci. Data 13 (9), 4349–4383.

Narama, C., Daiyrov, M., Tadono, T., Yamamoto, M., Kääb, A., Morita, R., Ukita, J., 2017. Seasonal drainage of supraglacial lakes on debris-covered glaciers in the Tien Shan Mountains, Central Asia. Geomorphology 286, 133–142.

Nie, Y., Sheng, Y., Liu, Q., Liu, L., Liu, S., Zhang, Y., Song, C., 2017. A regional-scale assessment of Himalayan glacial lake changes using satellite observations from 1990 to 2015. Remote Sens. Environ. 189, 1–13.

Nuimura, T., Fujita, K., Yamaguchi, S., Sharma, R.R., 2012. Elevation changes of glaciers revealed by multitemporal digital elevation models calibrated by GPS survey in the Khumbu region, Nepal Himalaya, 1992-2008. J. Glaciol. 58 (210), 648–656.
Otsu, N., 1979. A threshold selection method from gray-level histograms. IEEE Trans. Syst. Man Cybern. 9 (1), 62–66.
Palazzi, E., Von Hardenberg, J., Provenzale, A., 2013. Precipitation in the Hindu-Kush Karakoram Himalaya: observations and future scenarios. J. Geophys. Res.-Atmos. 118 (1), 85–100.
Panday, P.K., Bulley, H., Haritashya, U., Ghimire, B., 2011. Supraglacial Lake classification in the Everest region of Nepal Himalaya. Geospat. Tech. Manag. Environ. Resour. 86–99.
Qayyum, N., Ghuffar, S., Ahmad, H.M., Yousaf, A., Shahid, I., 2020. Glacial lakes mapping using multi satellite PlanetScope imagery and deep learning. ISPRS Int. J. Geo Inf. 9 (10), 560.
Qiao, L., Mayer, C., Liu, S., 2015. Distribution and interannual variability of supraglacial lakes on debris-covered glaciers in the Khan Tengri-Tumor Mountains, Central Asia. Environ. Res. Lett. 10 (1), 014014.
Racoviteanu, A.E., Nicholson, L., Glasser, N.F., 2021. Surface composition of debris-covered glaciers across the Himalaya using linear spectral unmixing of Landsat 8 OLI imagery. Cryosphere 15 (9), 4557–4588.
Racoviteanu, A.E., Nicholson, L., Glasser, N.F., Miles, E., Harrison, S., Reynolds, J.M., 2022. Debris-covered glacier systems and associated glacial lake outburst flood hazards: challenges and prospects. J. Geol. Soc. 179 (3), jgs2021-084.
Reynolds, J.M., 2000. On the formation of supraglacial lakes on debris-covered glaciers. Debris-covered glaciers.
RGI 7.0 Consortium, 2023. Randolph Glacier Inventory - A Dataset of Global Glacier Outlines, Version 7.0. Boulder, Colorado USA. NSIDC: National Snow and Ice Data Center. https://doi.org/10.5067/f6jmovy5navz. Online access: doi:10.5067/f6jmovy5navz.
Richardson, S.D., Reynolds, J.M., 2000. An overview of glacial hazards in the Himalayas. Quat. Int. 65, 31–47.
Rounce, D.R., Hock, R., McNabb, R.W., Millan, R., Sommer, C., Braun, M.H., Shean, D.E., 2021. Distributed global debris thickness estimates reveal debris significantly impacts glacier mass balance. Geophys. Res. Lett. 48 (8), e2020GL091311.
Sakai, A., Fujita, K., 2010. Formation conditions of supraglacial lakes on debris-covered glaciers in the Himalaya. J. Glaciol. 56, 177–181.
Sakai, A., Takeuchi, N., Fujita, K., Nakawo, M., 2000. Role of supraglacial ponds in the ablation process of a debris-covered glacier in the Nepal Himalayas. IAHS 119–132.
Scherler, D., Bookhagen, B., Strecker, M.R., 2011. Spatially variable response of Himalayan glaciers to climate change affected by debris cover. Nat. Geosci. 4 (3), 156–159.
Scherler, D., Hendrik, W., Noel, G., 2018a. Supraglacial Debris Cover. V. 1.0. GFZ Data Services.
Scherler, D., Wulf, H., Gorelick, N., 2018b. Global assessment of supraglacial debris-cover extents. Geophys. Res. Lett. 45 (21), 11–798.
Sharma, P., Partap, T., 1994. Population, poverty, and development issues in the Hindu Kush-Himalayas. Dev. Poor Mt. Areas 61–78.
Shean, D., Bhushan, S., Montesano, P., Rounce, D., Arendt, A., Osmanoglu, B., 2020. A systematic, regional assessment of High Mountain Asia Glacier Mass Balance. Front. Earth Sci. 7.
Shugar, D.H., Burr, A., Haritashya, U.K., Kargel, J.S., Watson, C.S., Kennedy, M.C., Bevington, A., Betts, R., Harrison, S., Strattman, K., 2020. Rapid worldwide growth of glacial lakes since 1990. Nat. Clim. Chang. 10 (10), 939–945.
Steiner, J.F., Buri, P., Miles, E.S., Ragettli, S., Pellicciotti, F., 2019. Supraglacial ice cliffs and ponds on debris-covered glaciers: spatio-temporal distribution and characteristics. J. Glaciol. 65 (252), 617–632.
Taylor, C.J., Carr, J., Rounce, D., 2021. Spatiotemporal supraglacial pond and ice cliff changes in the Bhutan–Tibet border region from 2016 to 2018. J. Glaciol. 1–13.
Thakuri, S., Salerno, F., Smiraglia, C., Bolch, T., D'Agata, C., Viviano, G., Tartari, G., 2014. Tracing glacier changes since the 1960s on the south slope of Mt. Everest (central Southern Himalaya) using optical satellite imagery. Cryosphere 8 (4), 1297–1315.
Thompson, S.S., Benn, D.I., Dennis, K., Luckman, A., 2012. A rapidly growing moraine-dammed glacial lake on Ngozumpa Glacier, Nepal. Geomorphology 145, 1–11.
Thompson, S., Benn, D.I., Mertes, J., Luckman, A., 2016. Stagnation and mass loss on a Himalayan debris-covered glacier: processes, patterns and rates. J. Glaciol. 62 (233), 467–485.
Wang, X., Guo, X., Yang, C., Liu, Q., Wei, J., Zhang, Y., Liu, S., Zhang, Y., Jiang, Z., Tang, Z., 2020. Glacial lake inventory of high-mountain Asia in 1990 and 2018 derived from Landsat images. Earth Syst. Sci. Data 12 (3), 2169–2182.
Wang, S., Peppa, M.V., Xiao, W., Maharjan, S.B., Joshi, S.P., Mills, J.P., 2022. A second-order attention network for glacial lake segmentation from remotely sensed imagery. ISPRS J. Photogramm. Remote Sens. 189, 289–301.
Wangchuk, S., Bolch, T., 2020. Mapping of glacial lakes using Sentinel-1 and Sentinel-2 data and a random forest classifier: Strengths and challenges. Sci. Remote Sens. 2, 100008.
Watson, C.S., Quincey, D., Carrivick, J., Smith, M., 2016. The dynamics of supraglacial ponds in the Everest region, central Himalaya. Glob. Planet. Chang. 142, 14–27.
Watson, C.S., King, O., Miles, E.S., Quincey, D.J., 2018. Optimising NDWI supraglacial pond classification on Himalayan debris-covered glaciers. Remote Sens. Environ. 217, 414–425.
Wendleder, A., Schmitt, A., Erbertseder, T., D'Angelo, P., Mayer, C., Braun, M.H., 2021. Seasonal evolution of Supraglacial Lakes on Baltoro glacier from 2016 to 2020. Front. Earth Sci. 9, 725394.
Wessels, R.L., Kargel, J.S., Kieffer, H.H., 2002. ASTER measurement of supraglacial lakes in the Mount Everest region of the Himalaya. Ann. Glaciol. 34, 399–408.
Xu, X., Liu, L., Huang, L., Hu, Y., 2024. Combined use of multi-source satellite imagery and deep learning for automated mapping of glacial lakes in the Bhutan Himalaya. Sci. Remote Sens. 10, 100157.
Yao, T., Bolch, T., Chen, D., Gao, J., Immerzeel, W., Piao, S., Zhao, P., 2022. The imbalance of the Asian water tower. Nat. Rev. Earth Environ. 3 (10), 618–632.
Yuan, J., Chi, Z., Cheng, X., Zhang, T., Li, T., Chen, Z., 2020. Automatic extraction of supraglacial lakes in southwest greenland during the 2014–2018 melt seasons based on convolutional neural network. Water 12, 891.
Zeller, L., McGrath, D., McCoy, S.W., Jacquet, J., 2024. Seasonal to decadal dynamics of supraglacial lakes on debris-covered glaciers in the Khumbu region, Nepal. Cryosphere 18 (2), 525–541.
Zhang, E., Liu, L., Huang, L., Ng, K.S., 2021. An automated, generalized, deep- learning-based method for delineating the calving fronts of Greenland glaciers from multi-sensor remote sensing imagery. Remote Sens. Environ. 254, 112265.